6

The oceans

William S. Kessler

6.1 INTRODUCTION

There is a very wide variety of intraseasonal variability (ISV) in the oceans, due to many different processes beyond forcing by tropical intraseasonal winds and heat fluxes. The main focus of this chapter, however, is on the upper ocean response to the tropical atmospheric ISV that is discussed in the other chapters of this book and is most germane in this context. The prominent oceanic ISV signatures generated by other mechanisms (largely intrinsic to the ocean), and those found in other regions are briefly reviewed in Section 6.7.

Episodic wind events on intraseasonal timescales affect the ocean through three main mechanisms: increased evaporation, the generation of equatorial jets and waves that produce advective changes remotely, and enhanced mixing and entrainment. As Webster and Lukas (1992) note, these responses are proportional to the windspeed u, u^2, and u^3 respectively, and therefore depend very differently on the background wind and the structure of its variance. Much of the forcing by tropical intraseasonal oscillations (TISO) occurs over the warm pools of the Indian and west Pacific Oceans where the thermocline is usually deeper than the mixed layer. Thus, the near-surface density structure is relatively unconstrained by large-scale ocean dynamics and can easily be modulated by the winds and the heat and moisture fluxes due to the ISV, providing the opportunity for air–sea feedbacks, non-linear effects, and the retention of an oceanic memory of previous forcing. The dynamic response depends on the thickness of the accelerating layer, which is a function both of the background stratification and of local precipitation and mixing. Thus a principal focus of this chapter (Sections 6.2 and 6.3) is the factors controlling the upper ocean stratification under rapidly changing windspeed and precipitation sufficient for salinity variation to determine the mixed layer depth. The correlation of ISV of solar short-wave forcing with the wind fluctuations can also lead to significant

W. K. M. Lau and D. E. Waliser (eds), *Intraseasonal Variability in the Atmosphere–Ocean Climate System*.

effects on mixed layer temperature structure, with a variety of consequences (Section 6.5 and Chapter 7).

Because most of the work on oceanic ISV has been done in the Pacific, while the Indian Ocean is relatively poorly sampled, the processes of the oceanic response are described in the Pacific context, and factors specific to the Indian Ocean are discussed in Section 6.6.

Much of the interest in tropical ISV in recent years has concerned its possible interaction with the El Niño Southern Oscillation (ENSO) cycle, which has been a controversial element of the debate over the nature of ENSO. While coupled models without realistic ISV have been successful in reproducing aspects of ENSO statistics, it remains in question whether ENSO is a disturbance to a stable background state, in which case an initiating perturbation would be required, or is a self-sustained mode on an unstable background. After satellite sampling established the occurrence of strong Madden–Julian Oscillation (MJO) events penetrating into the western Pacific during the onset stages of El Niño, several mechanisms have been proposed by which rectification of intraseasonal forcing in the ocean could interact constructively with the ENSO cycle; these are discussed in Section 6.5. (see also Chapters 9 and 12 for additional discussion of ISV–ENSO interactions).

6.2 HEAT FLUXES

Intraseasonal ocean–atmosphere heat fluxes are discussed in several other parts of this book, especially Chapters 7, 10, and 11; this section will focus on changes in the structure of the ocean in response to those fluxes, especially within the west Pacific warm pool that has been extensively studied (see Godfrey *et al.*, 1998, for a review of the Tropical Ocean Global Atmosphere (TOGA) Coupled Ocean–Atmosphere Response Experiment (COARE) program). The west Pacific warm pool differs from most other open-ocean regions because its heavy precipitation and generally weak winds mean that the seasonal background mixed layer depth is often controlled by salinity stratification. Net precipitation minus evaporation over the warm pool is $1–2\,\mathrm{m\,yr^{-1}}$ (Anderson *et al.*, 1996), leading to low surface salinity that plays a major role in determining the vertical stability of the warm pool. As a result, the thick warm layer above the thermocline can be split by a halocline, and its lower part thereby uncoupled from surface forcing. Much of the precipitation occurs during convection associated with TISO events, which also produce strong shortwave and windspeed variability as convective systems pass across the region (see Figure 1.2 and Chapter 7).

6.2.1 Salinity and the barrier layer

The isothermal layer beneath the halocline has become known as the "barrier layer" (Lukas and Lindstrom, 1991; Sprintall and Tomczak, 1992) since it inhibits the communication between the surface and the thermocline that dominates sea surface temperature (SST) change in the central and eastern equatorial Pacific (e.g., Kessler and McPhaden, 1995b; Zhang, 2001). A thin mixed layer tends to

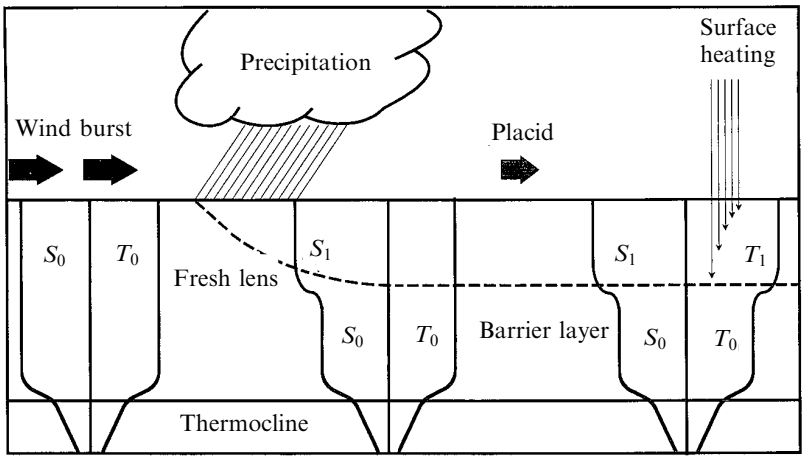

Figure 6.1. Schematic diagram showing the Lukas–Lindstrom "barrier layer" theory. During a strong wind burst, the surface mixed layer extends down to the top of the thermocline. Following the wind burst, the additional buoyancy from precipitation and strong surface heating acts to form a relatively warm and fresh thin surface layer. Below this thin layer is a strong halocline, which effectively decouples the surface forcing from the deeper waters. Further heating is trapped to vertical mixing above the barrier formed by the halocline.
After Anderson *et al.* (1996).

trap surface fluxes of heat and momentum within it, enhancing both SST variability in response to heat fluxes and the acceleration of surface currents in response to winds. Figure 6.1 shows a schematic of barrier layer formation and erosion (Anderson *et al.*, 1996). Under strong winds, the upper layer can become well-mixed down to the deep thermocline of the west Pacific (typically 150 m; e.g., Figure 6.2). Following heavy precipitation, as long as the winds aren't strong enough to mix it away, a fresh lens can cap the top of the isothermal layer (Figure 6.1, middle). If this stratification is maintained, subsequent surface heating under clear skies will mostly occur within this relatively thin layer (≤ 50 m), because the short-wave attenuation with depth is exponential (Figure 6.1, right) and not be mixed over the entire above-thermocline layer as would generally occur in other regions. (However, if the surface layer is very thin, some radiation will penetrate into the barrier layer (see next section).) Because the halocline inhibits mixing, and because additional heating enhances its stability, the barrier layer tends to persist until winds (often in the form of intraseasonal westerlies) are strong enough to mix it away. Model experiments based on the situation during TOGA COARE suggest that the observed stratification produces close to the maximum possible SST: increased precipitation or weaker winds would result in a shallower mixed layer that would lose heat through its base by penetrative radiation, whereas decreased precipitation or stronger winds would lead to fewer barrier layer occurrences and thus more entrainment cooling (Anderson *et al.*, 1996). Recent work has suggested other mechanisms that can produce or intensify barrier layers on intraseasonal timescales. For example, since west Pacific surface salinity is lower than that further east, if a

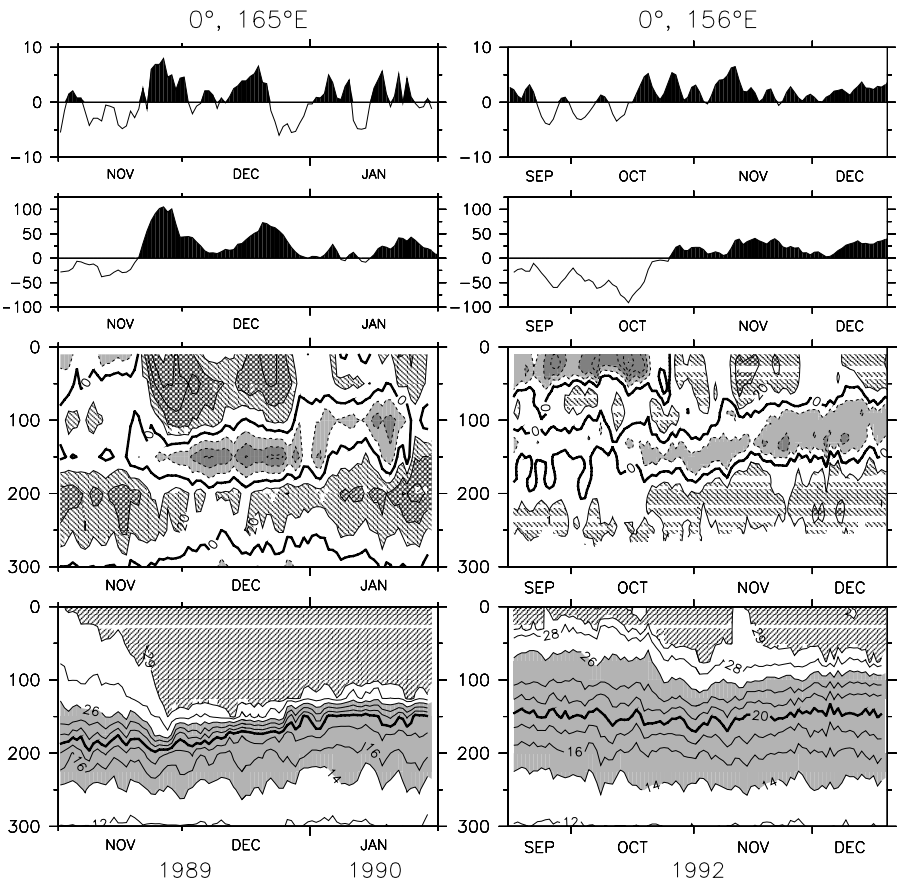

Figure 6.2. Zonal wind (*top*), 10-m zonal current (*upper middle*), zonal current (*lower middle*), and temperature (*bottom*) at 0°, 165°E during 1989–1990 (*left panels*) and at 0°, 156°E during 1992 (*right panels*). In the upper panels westerly winds and eastward currents are shaded. In the lower middle panels hatching indicates eastward currents, gray-shading westward currents, with a contour interval of 20 cm s^{-1}. In the bottom panels, hatching indicates temperatures greater than 29°C, and gray-shading indicates the thermocline with temperatures between 14°C and 26°C.

rain-produced halocline and westerly winds lead to a surface-intensified eastward jet (see Section 6.3), then the resulting shear will tend to tilt the zonal salinity gradient by causing the fresh lens to run over the saltier eastern layer (Roemmich *et al.*, 1994; Cronin and McPhaden, 2002). Similarly, Ekman convergence in response to westerly winds can bring fresher northern hemisphere surface water to the equator (Cronin and McPhaden, 2002). However it is caused, the existence of a barrier layer enhances the local ocean response to both heat and momentum fluxes by concentrating it in a thin surface layer.

6.2.2 A 1-D heat balance?

Numerous studies have shown that, although advection can on occasion be important in determining near-surface temperature change, a 1-D balance dominated by surface fluxes is the principal influence determining warm pool SST variability (McPhaden and Hayes, 1991; Webster and Lukas, 1992; McPhaden *et al.*, 1992; Sprintall and McPhaden, 1994; Anderson *et al.*, 1996; Cronin and McPhaden, 1997; Shinoda and Hendon, 1998, 2001; Zhang and McPhaden, 2000). The principal surface flux terms on intraseasonal timescales are latent heat flux, which varies mostly due to windspeed since the SST is always high (Cronin and McPhaden, 1997), and short-wave radiation, varying mostly due to the thick cloudiness of convective systems; both of these have strong signatures as TISO events pass across the region (Shinoda *et al.*, 1998). Since highest wind speeds occur during westerly wind bursts (Weller and Anderson, 1996; Zhang and McPhaden, 2000), which are themselves associated with the convective phase of TISOs (Zhang, 1996; Shinoda and Hendon, 2002), the short-wave and latent heat flux terms are approximately in phase on intraseasonal timescales (Figure 7.1), and a convective event produces strong cooling (McPhaden *et al.*, 1988, 1992; Ralph *et al.*, 1997; Zhang and McPhaden, 2000). Figure 6.3 shows episodes of cooling under the intraseasonal

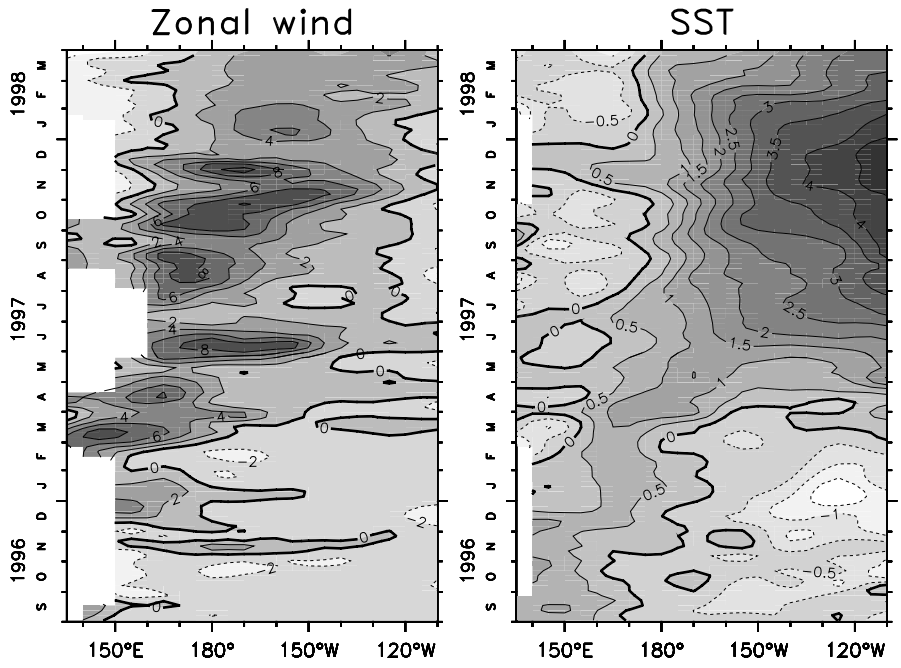

Figure 6.3. Zonal wind (*left*) and SST (*right*) anomalies along the equator, based on data from Tropical Atmosphere Ocean (TAO) moorings. Dark shading and solid contours indicate westerly wind and high SST anomalies. Contour intervals and $2\,\mathrm{m\,s^{-1}}$ and 0.5°C.

westerly wind bursts during the growth of the 1997/1998 El Niño. The implications of the net cooling of the far western Pacific as a result of TISO events will be discussed in Section 6.5. In addition to attempts to directly estimate the heat balance terms, several types of overview evidence indicate the dominance of surface flux forcing in the upper layer intraseasonal heat balance. First, the meridional scale of cooling under strong westerly winds has been observed to have the relatively broad scale of the wind, rather than that of the ocean dynamical response, which is more closely trapped to the equator (Ralph *et al.*, 1997; Shinoda and Hendon, 2001). Second, temperature anomalies subsequent to surface fluxes associated with the MJO are observed to propagate downwards, and are not in phase with deeper temperature variability (Zhang, 1997).

Entrainment from below might also contribute to SST change in a 1-D balance, and this has been considered by several investigators, although it cannot be measured directly and is often inferred from the residual of other terms (e.g., McPhaden and Hayes, 1991; Cronin and McPhaden, 1997). Entrainment could be fostered by dynamical processes like Ekman-divergence-caused upwelling bringing cooler water within the reach of wind mixing, as occurs in the eastern Pacific, or due to wind mixing itself against shallow stratification (e.g., mixing away a halocline and exposing a cooler barrier layer as would occur in Figure 6.1). The thickness of the warm layer and its frequent stabilization by salinity make entrainment relatively ineffective at cooling the SST in the west Pacific warm pool, most of the time (Meyers *et al.*, 1986; McPhaden and Hayes, 1991; Eldin *et al.*, 1994). Exceptions have been noted, however. Cronin and McPhaden (1997) used a steady-state turbulence model to show that entrainment was a cooling tendency during a period of shallow pycnocline early in COARE, though it was apparently not the main reason for changes in pycnocline depth. Sprintall and McPhaden (1994) found that during La Niña conditions in 1988/1989, with stronger than normal trades and weak rainfall at 0°, 165°E, there was no barrier layer. In this situation, SST changes were significantly influenced by upwelling (downwelling) in response to easterly (westerly) wind anomalies, much as occurs in the eastern and central Pacific. Although entrainment is generally a cooling term, salinity stratification can result in entrainment warming. Under low wind and clear-sky conditions, a very shallow halocline can lead to heating of the barrier layer by penetrative radiation (which remains stable because of the low surface salinity). With the turn to the cloudy–windy phase, surface flux cooling reduces the vertical stability while wind mixing strengthens; the result can be that entrainment produces heating of the surface (Anderson *et al.*, 1996; Shinoda and Hendon, 1998; Schiller and Godfrey, 2003).

6.2.3 The role of advection

The importance of intraseasonal heat advection in the warm pool has been controversial. On one hand, as noted above, many investigators have concluded that a 1-D balance represents the dominant physics; these arguments appear reasonable since mean SST gradients in the warm pool are small. However, several examples have demonstrated that advection can be a significant contributor to the

heat balance in certain cases, involving different processes under both easterly and westerly winds. Despite the uniformity of mean SST in the warm pool, remnants of anomalous SST patches due to preceding conditions can leave significant, if transient, gradients for currents to work on, and as discussed in Section 6.3, equatorial currents can spin up rapidly in response to intraseasonal wind reversals. Two examples from the COARE experiment suggest the range of possibilities. During the early part of COARE in October 1992, cooler SSTs lay at, and west of, the 156°E mooring, presumably the residual of a westerly wind event in September. Moderate easterly winds (Figure 6.2, top right) spun up a strong westward surface current (Figure 6.2, right middle) that produced advective warming of about 1°C during the first three weeks of October (Cronin and McPhaden, 1997). Two months later, the strongest intraseasonal westerly event during COARE occurred in late December 1992, with stresses as high as $0.4\,\mathrm{N\,m^{-2}}$ (Weller and Anderson, 1996). Currents spun up by the December winds were well observed by surface drifters, which are drogued to move with the current at a 15-m depth and had been seeded extensively around the region (Ralph *et al.*, 1997). During the event, drifters within at least 2°S to 2°N converged onto the equator and accelerated eastward. The surface jet extended at least to 180°, and was about 300 km wide (Figures 7.10 and 7.11). Surface layer cooling under the strong winds was substantial, with a temperature drop of as much as 1°C along the drifter trajectories. Ralph *et al.* (1997) found that this heat loss resulted in a positive SST gradient with SSTs warmer by at least 1°C near 180° than at 145°E, and consequently eastward advection was a cooling term in the eastern part of the warm pool. They noted that the strong latent heat and shortwave cooling under the cloudy-westerly phase of TISO events means that eastward surface currents tend to be correlated with positive SST gradients ($\overline{u'T'_x} > 0$). This correlation suggests that long-term mean zonal advection is not negligible despite the small mean SST gradients, and that the time-average effect of TISO winds and clouds is cooling at the east edge of the warm pool (Ralph *et al.,* 1997). Both these examples contradict the conventional idea that mean SST advection along the equator is due to the westward mean South Equatorial Current (SEC) working on the mean negative SST gradient, and indicate the potential for ISV to produce low-frequency changes in SST (see Section 6.5).

6.3 VERTICAL STRUCTURE UNDER WESTERLY WINDS

The complex and rapidly-varying vertical structure of west Pacific zonal currents has been noticed from the earliest cruises in the region (Hisard *et al.*, 1970). During a cruise along 170°E in March 1967, trade winds prevailed and the equatorial currents had a two-layer structure, with a westward SEC above 60 m depth, and an eastward Equatorial Undercurrent (EUC) below. This is typical of the trade wind regime of the central Pacific; in the mean it has been shown to be the result of a directly wind-forced frictional current in the surface layer, with a baroclinic pressure gradient due to thermocline tilt producing an eastward current below (McPhaden and Taft, 1988). In the following month, a westerly wind burst had occurred, and Hisard *et al.*

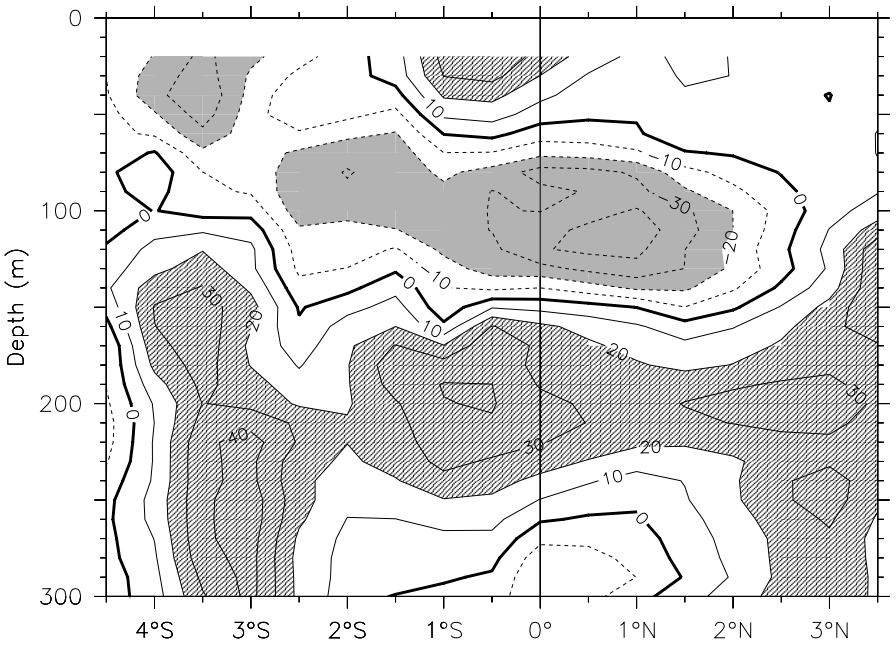

Figure 6.4. Zonal current example illustrating the subsurface westward jet (SSWJ) sandwiched between a frictional surface eastward current and the eastward EUC at 200 m. Hatching and solid contours indicate eastward current, gray-shading and dashed contours indicate westward current. The contour interval is 10 cm s^{-1}. The measurements were made by shipboard acoustic doppler current profiler (ADCP) along 156°E during 8–11 December, 1992, from the *R/V Le Noroit*. Only data obtained while the ship was on-station was used to construct the section.

(1970), observed a three-layer structure, with eastward flow above 60 m depth, westward flow from 60 m to 175 m, and the eastward EUC below that (similar to Figure 6.4); these have become known as "reversing jets" and the sandwiched westward current has been called the subsurface westward jet (SSWJ).

Since the Hisard *et al.* (1970) study, there have been numerous reports of such reversing jets in the western equatorial Pacific (McPhaden *et al.*, 1988, 1990, 1992; Delcroix *et al.*, 1993; Cronin *et al.*, 2000). In general, they are not found in the central or eastern Pacific, despite decades-long moored velocity time series at several locations; however, Weisberg and Wang (1997) showed one example of a brief reversing jet at 170°W during the eastwardmost penetration of westerly winds in January 1992, at the height of the El Niño of that year. It seems likely that a deep thermocline and a thick, weakly stratified surface layer is necessary for the complex structure of velocity to exist, thus restricting the reversing jets to the warm pool, except occasionally during El Niños when these conditions spread eastward.

It was soon recognized that the surface eastward current associated with the

reversing jets was an example of a Yoshida Jet (Yoshida, 1959). A Yoshida Jet has the simple, accelerating balance:

$$u_t - fv = \tau^x/h \tag{6.1a}$$

$$fu = -p_y \tag{6.1b}$$

$$p_t + hv_y = 0 \tag{6.1c}$$

where (u, v) are the zonal and meridional velocity components, f is the Coriolis parameter, τ^x is the zonal wind stress, h is the thickness of the accelerating layer, and p is the pressure (both τ and p have been divided by the density for simplicity of notation). The zonal jet that is the solution to (6.1) decays exponentially away from the equator with a meridional scale of the equatorial Rossby radius (typically 300 km). Away from the equator, meridional transport in (6.1a) is approximately Ekman convergence (for westerly winds), which feeds the accelerating zonal jet, and produces equatorial downwelling (6.1c) that provides the meridional pressure gradient to geostrophically balance the jet (6.1b). For a westerly wind burst magnitude of $7.5\,\mathrm{m\,s^{-1}}$ (e.g., Figure 6.2, top) the stress anomalies would be about $0.1\,\mathrm{N\,m^{-2}}$. Taking a 100 m layer thickness, the zonal acceleration at the equator indicated by (6.1a) is of the order of $10\,\mathrm{cm\,s^{-1}\,day^{-1}}$, comparable to observations under these conditions, and indicating that a very rapid current can be spun up within the timescale of a westerly wind burst (McPhaden *et al.*, 1988, 1992; Ralph *et al.*, 1997; Cronin *et al.*, 2000). Yoshida Jets appear to be a common and robust feature of the west Pacific under westerly wind bursts, and are frequently observed (McPhaden *et al.*, 1990; Delcroix *et al.*, 1993). Since the Yoshida balance does not consider zonal variability, the jet is assumed to occur everywhere under the wind; an unresolved question concerns the possible convergence at the east edge of the jet (Richardson *et al.*, 1999; Cronin and McPhaden, 2002; Lengaigne *et al.*, 2002).

Cronin *et al.* (2000) diagnosed the zonal momentum terms in the COARE region during March 1992–April 1994. Figure 6.5, from that paper, shows that near-surface zonal acceleration was nearly in phase with the wind and that the jet reaches maximum velocity within about 3 days from the peak of the wind. Examples of rapid acceleration of surface currents under westerly wind bursts are common (e.g., Figure 6.2). One model of the response to impulsive forcing simplified the situation by assuming linear, frictional dynamics in a homogeneous mixed layer above a sharp thermocline (McPhaden *et al.*, 1988). With switched-on zonal-wind forcing, their solution for the shear flow was a parabolic velocity profile accelerating in the direction of the wind, maximum at the surface and decaying to zero at the base of the mixed layer. With a vertical eddy viscosity estimated from observed shear profiles, the shear profile set up within several days.

The Yoshida Jet would accelerate without bound except that the zonal pressure gradient term, omitted from (6.1a), becomes important in days to weeks and results in equatorial Kelvin and Rossby waves being emitted from the edges of the wind patch (McCreary, 1985). (The meridional profile of the wind determines the mix of Kelvin and Rossby waves; see Richardson *et al.*, 1999.) The Kelvin wave part of the

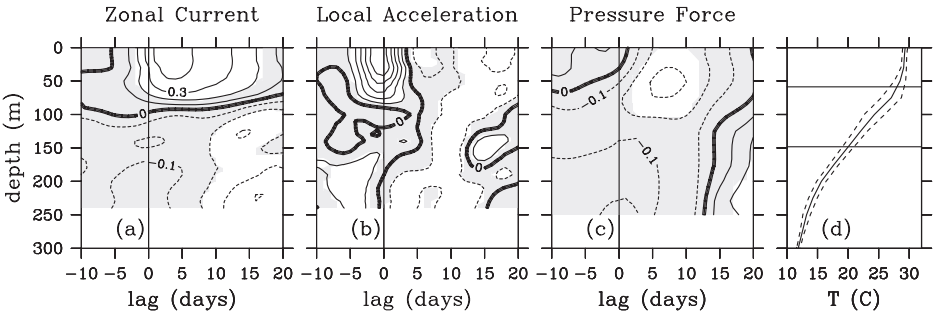

Figure 6.5. Lagged correlation between local zonal wind stress and (a) zonal current, (b) local zonal current acceleration, and (c) zonal pressure gradient force as a function of depth, at 0°, 156°E. A positive lag implies that wind stress variability occurs prior to the respective variable anomaly. (d) Mean temperature and its standard deviation envelope at 0°, 156°E. The two horizontal lines show the mean depths of the 28°C and 20°C isotherms, which define the surface, intermediate and EUC layers. Correlations that are not significant at the 90% confidence level are shaded. The contour interval is 0.1.
After Cronin *et al.* (2000).

response has no effect west of the wind patch but carries a downwelling signal to the east, such that the thermocline tilts down to the east under the (westerly) wind patch and is flat from its eastern edge to the back of the advancing wave. The Rossby part of the response has no role east of the patch but carries an upwelling signal westward. If a westerly wind remains steady (and ocean boundaries are unimportant), the fully-adjusted solution has a flat, upwelled thermocline to the west, a downward slope under the wind, and a flat, downwelled thermocline to the east. Under the wind patch itself, the vertically-integrated zonal pressure gradient comes to Sverdup balance with the wind stress, and the acceleration stops; in effect the waves carry the wind-input momentum away from the forcing region. The result is a downwind jet at the surface, decaying with depth, and a pressure-gradient-driven upwind current below, as the frictional influence declines with depth. For steady easterly winds, this two-layer structure describes the mean situation in the central Pacific, with a westward SEC at the surface, and EUC beneath. (For discussion of non-linearities associated with these circulations, see, among many others, Philander and Pacanowski, 1980; Johnson and McPhaden, 1993a, b; Johnson and Luther, 1994; Yu and Schopf, 1997; Zhang and Rothstein, 1998; Cronin *et al.*, 2000; Lengaigne *et al.*, 2002; Kessler *et al.*, 2003). The key questions for westerly wind bursts, therefore, are the timescale on which the waves establish the pressure gradient and how the vertical structure that allows *three* stacked jets to exist is set up.

The pressure gradient timescale depends primarily on the width of the wind patch compared to the propagation time of the waves. For typical westerly wind burst forcing with fetch of a few thousand kilometers, and first baroclinic mode Kelvin waves with speeds of 2–3 $\mathrm{m\,s^{-1}}$, the pressure gradient setup takes about 10 days, which is borne out by observation (Figure 6.5(c), and see Cronin *et al.*, 2000).

Model experiments with idealized winds have shown a strong sensitivity of the ocean response to the wind fetch and zonal profile (Richardson *et al.*, 1999).

Yoshida dynamics alone can only set up shear of one sign and therefore only two stacked jets. The reversing jets observed under westerly wind bursts, however, demonstrate the possibility of a surface eastward Yoshida Jet, an eastward EUC in the center of the thermocline, and a westward flow (the reversing jet or SSWJ) in the weakly stratified upper thermocline between them (Figures 6.2 and 6.4). In fact, Figure 6.2 shows that a quite complicated vertical structure can occur with rapid wind changes; note that the zonal current at 156°E in September and early October, 1992, under easterly winds, has a surface westward current varying in phase with the wind, a subsurface eastward current near 80 m that is apparently driven by the shallow pressure gradient response to the easterlies, a remnant of a SSWJ at 130 m generated by the early September westerlies, and the EUC at 240 m below that. This suggests that the relatively diffuse west Pacific thermocline can support pressure gradient reversals in the vertical (Cronin *et al.*, 2000). Observations show examples of the EUC flowing nearly undisturbed during the occurrence of significant westerly winds with the formation of a Yoshida Jet and SSWJ lasting for several months (e.g., Figure 6.2, right-hand panels), and conversely of a reversed pressure gradient extending into the central thermocline and slowing the EUC as the SSWJ develops (McPhaden *et al.*, 1992; see Figure 6.2, left-hand panels). On average, the pressure gradient and zonal current at EUC-level are weakly correlated with local zonal winds with a lag of about 15 days (Cronin *et al.*, 2000; see also Figure 6.5(a, c)). One can imagine that the different responses depend sensitively on the preexisting stratification and current structure: in particular the thickness of the SEC and how far it extends into the thermocline, and whether the upper thermocline above the EUC can adjust to produce a pressure gradient to bring the Yoshida Jet to steady state, and thereby create a SSWJ, without involving the lower isotherms. Model experiments to try to isolate these effects have been performed by Zhang and Rothstein (1998) and Richardson *et al.* (1999).

This raises the deeper issue of what determines the vertical structure of ocean adjustment to time-varying winds. On the basin-scale at low frequency (say six months or more), the entire thermocline slope adjusts to Sverdrup balance with the wind stress (McPhaden and Taft, 1988). In the eastern Pacific, where the thermocline is sharp and shallow and the winds are relatively steady easterlies that provide, via upwelling, for quick communication of thermocline anomalies to the surface, there is little opportunity for a complex vertical structure to occur. But in the warm pool, where the upper layer can be more than 100 m thick, the thermocline can extend over 200 m or more, and the winds commonly change sign in a month or less, a more elaborate structure is possible. For example, Zhang (1997) noted that although intraseasonal temperature variability at 0°, 165°E is large down to at least 300 m, the signal is incoherent across about 75 m depth. The factors setting the vertical scales of these reversals presumably are related to the pre-existing stratification, but this is not well understood.

6.4 REMOTE SIGNATURES OF WIND-FORCED KELVIN WAVES

The propagation of equatorial Kelvin waves is so efficient at carrying wind-forced signals eastward along the equator that the first recognition of intraseasonal timescales in the tropical Pacific Ocean was in sea level records along the coast of the Americas (Enfield and Lukas, 1983). Spillane *et al.* (1987) and Enfield (1987) documented coherent 30–70 day period coastal sea level variability from Peru to northern California. They quickly realized that nothing in the local winds could produce such a signal, and found a lag relation with west Pacific island sea levels that clearly showed the Kelvin wave propagation, at speeds of about $2.5\,m\,s^{-1}$. More recently, Hormazabal *et al.* (2002) made a similar diagnosis for sea level at 30°S on the Chilean coast (see also Clarke and Ahmed (1999), for an analysis of the role of the continental shelf in determining the phase speed of coastal propagation).

Since the TAO mooring array (Hayes *et al.*, 1991; McPhaden, 1995) has provided adequate temporal resolution, observation of the prominent intraseasonal Kelvin waves has become routine. The Kelvin wave due to intraseasonal westerly wind events is seen as a thermocline downwelling that commonly can be 50 m or more (Figure 6.6), well east of the wind itself, and accompanied by an eastward surge of surface current that can be as large as $1\,m\,s^{-1}$. Their effects on SST in the central and eastern Pacific have been noted many times. Under some conditions, SST change at 140°W can be dominated by the intraseasonal zonal advection due to west Pacific Kelvin waves (Kessler *et al.*, 1995). Vecchi and Harrison (2000) stratified westerly wind bursts by location and by the low-frequency background state of ENSO. They showed that, on average, the largest east Pacific SST effects were found when equatorial westerlies occurred with climatologically-normal SST, not during El Niño events, apparently because zonal advection is more efficient at changing SST when a large background zonal gradient exists. The westerly-wind-driven Kelvin waves can also remotely modulate eastern Pacific SST through lowering the thermocline (Figure 6.6) and changing the effect of background upwelling on SST, which Zhang (2001) argued was the dominant mechanism (see also Belamari *et al.*, 2003). Giese and Harrison (1991) suggested that another possible SST effect could be due to the passage of a downwelling Kelvin wave, with a meridional scale of 2°–3°, accelerating the EUC and thereby increasing the shear with the surrounding SEC. In their model, the resulting amplification of the tropical instability waves (see Section 6.7.2) resulted in an equatorward heat flux that was as large as the zonal advection warming.

The TAO moorings have also allowed the vertical structure of the intraseasonal Kelvin waves to be dissected and diagnosed. McPhaden and Taft (1988) used moorings at 140°W, 125°W and 110°W, where there is little intraseasonal wind forcing, to show that the principal intraseasonal signals in zonal current, temperature, and dynamic height had characteristics of a remotely-forced first baroclinic mode Kelvin wave, with speed about $2.1\,m\,s^{-1}$, and that this variability had an amplitude as large as that of the annual cycle. They also commented that the dominant intraseasonal period observed in these oceanic variables was 60–90 days, longer than the apparent MJO forcing (see Section 6.5 for further discussion of this

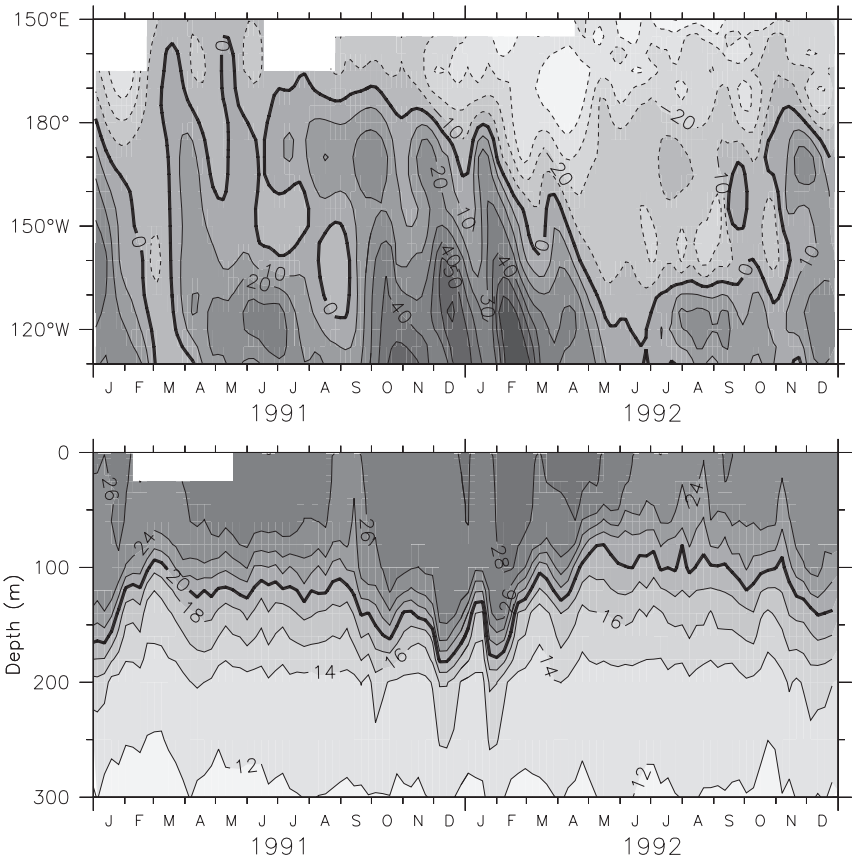

Figure 6.6. (*Top*) Anomalous depth of the 20°C isotherm along the equator. Dark shading indicates deep anomalies, with a contour interval of 10 m. The intraseasonal Kelvin waves are evident as tilted bands, especially during September 1991–February 1992. (*Bottom*) Temperature at 0°, 140°W. Dark shading indicates higher temperature, with a contour interval of 2°C. The 20°C isotherm is shown as the thick line. Kelvin waves arriving from the western Pacific produce the sharp downwelling events. For both panels, data comes from TAO moorings.

issue). Although their results suggested that the waves were approximately linear, the fact that the EUC speed is typically $1\,\mathrm{m\,s^{-1}}$ or more raised the question of mean current modifications of the wave modes. Johnson and McPhaden (1993b) analyzed time series of temperature and zonal current from moorings along 140°W and compared them with a meridionally-symmetric model that included an idealized mean flow comparable to the EUC, as well as a SEC centered near 3° latitude at the surface. Relatively little direct Doppler shifting was found, because the wave vertical scales are so much larger than those of the mean currents, and the main modifications to linear dynamics were the occurrence of a temperature amplitude

minimum on the equator and an amplification of the wave zonal currents below the EUC core (see also Lengaigne *et al.* (2002) who emphasized that Kelvin advection of the mean EUC was responsible for this). Both these effects were due to wave vertical advection of the background temperature and current fields. Considering these studies, a linear diagnosis of the remotely-forced Kelvin waves seems to be first order appropriate.

Theory suggests that many vertical Kelvin modes would be excited by the observed wind forcing, and several studies have noted evidence for modal structures. Busalacchi and Cane (1985) showed that while both the first and second vertical modes are a significant contribution to sea level variability in the eastern Pacific, higher modes are not. Giese and Harrison (1990) found that in an OGCM with a realistically-sloping equatorial thermocline, the second baroclinic mode Kelvin wave's surface currents would be amplified relative to that of the first mode, and would be the dominant velocity signal at the South American coast. Kutsuwada and McPhaden (2002) pointed out that during El Niño events, when the thermocline is flatter than usual, this effect would be moderated and the first baroclinic mode more prominent. They also showed evidence of upward phase propagation in the free-wave region, suggesting the formation of a downward beam of energy (McCreary, 1984). Kindle and Phoebus (1995) found that a model including three modes gave a better simulation of sea level at the American coast. Cravatte *et al.* (2003) showed evidence of energy transfer from the first to the second baroclinic mode for intraseasonal Kelvin waves during 1992/1999. In light of these results suggesting the importance of at least the second baroclinic mode, the apparent success of single-active-layer (reduced gravity) models in simulating much of the observed wave-mediated variability (Metzger *et al.*, 1992; Wu *et al.*, 2000) is puzzling. Kessler and McPhaden (1995a) examined the signatures of the first four baroclinic modes in thermocline depth at 140°W and found that although in a strict modal decomposition two modes were needed, in fact reasonable choices of reduced gravity (thus single-mode) parameters gave a very similar solution, at least in the central Pacific not too far from the forcing region. The reason is that the typical choice for wave speed in the reduced gravity models ($c = 2.5\,\mathrm{m\,s^{-1}}$) is appropriate to a true first mode with about 250 m thickness (where $c^2 = g'h$, with g' the reduced gravity and h the layer thickness), but in fact these models are often taken to have h be a realistic thermocline depth of about 150 m. These choices therefore artificially pump up the mode-one amplitude, and thereby compensate to produce a fairly realistic representation of the total Kelvin signal (Kessler and McPhaden, 1995a).

Although Kelvin waves propagate non-dispersively with a simple velocity and thermocline depth anomaly structure that has u and h in phase, they can produce much more complex phasing of SST variability. Indeed, Kessler and McPhaden (1995a) had noted, but could not explain, the intraseasonal warming and cooling events that occurred nearly simultaneously over a wide longitude range during the onset and decay of the El Niño of 1991/1992. McPhaden (2002) interpreted this by showing that while Kelvin wave zonal advection dominates the intraseasonal SST balance in the central Pacific, vertical advection and entrainment are more important in the east where the thermocline is very shallow. If Kelvin wave vertical velocity is

assumed to be due to thermocline motion ($w \approx dh/dt$), then upwelling leads the westward current anomaly by 1/4 of a cycle as the wave passes a point. Thus, the cooling due to upwelling also leads the cooling due to wave zonal advection of the mean SST gradient by 1/4 of a cycle. Depending on the relative importance of each of these processes to the SST balance at different longitudes, the phasing of SST due to intraseasonal Kelvin waves can appear to propagate in either direction or occur in phase. McPhaden (2002) showed that the growing dominance of vertical entrainment as the Kelvin wave propagates eastward led to the nearly simultaneous intraseasonal SST anomalies over a broad longitude range observed throughout the 1990s.

Although equatorial Kelvin waves can have arbitrary shape in (x, t), two factors combine to make the MJO fraction of ISV the dominant contribution to the oceanic Kelvin signal. First, since the ocean integrates the wind forcing along the Kelvin wave characteristics (Kessler *et al.*, 1995; Hendon *et al.*, 1998), organized, large-scale forcing is favored over more incoherent variability. Second, wind forcing that moves eastward will project more strongly onto the Kelvin mode (Weisberg and Tang, 1983), because it is partly resonant. Over the west Pacific warm pool, the MJO propagates east at a speed of about $5\,\mathrm{m\,s^{-1}}$ (Hendon and Salby, 1994; Shinoda *et al.*, 1998), which is comparable to the oceanic Kelvin speed (about $2.5\,\mathrm{m\,s^{-1}}$ for the first vertical mode). Hendon *et al.* (1998) noted that as the MJO speeds up east of the dateline, it gets ahead of the oceanic Kelvin wave; by about 130°W it is out of phase with the Kelvin current anomalies and thus serves to damp the wave.

In addition to the effects discussed in this section, intraseasonal Kelvin waves have also been related to the ENSO cycle and rectification mechanisms through a variety of processes. These will be discussed in Section 6.5.

6.5 EL NIÑO AND RECTIFICATION OF ISV

The question of a role for ISV, especially the MJO, in the ENSO cycle has been a hotly debated topic in the climate community (Zhang *et al.*, 2001), and no definitive resolution has thus far been reached (see Chapter 9). Although the intraseasonal signatures in the ocean during El Niños can be impressively large, comparable to the amplitude of the seasonal cycle or ENSO (e.g., Figure 6.6), a non-linear mechanism would be required to couple intraseasonal to lower frequencies, and this has been difficult to demonstrate. In addition, the usual indices of global MJO activity are uncorrelated with indices of the ENSO cycle (Slingo *et al.*, 1999; Hendon *et al.*, 1999), which has led some to argue that a systematic connection is unlikely. Nevertheless, the frequent observation of strong intraseasonal (especially MJO) variability in the western Pacific during the onset stage of recent El Niños (Gutzler, 1991; Kessler *et al.*, 1995; McPhaden, 1999; McPhaden and Yu, 1999; Zhang and Gottschalck, 2002) has generated a variety of speculation about this possibility. The spectacular failure of all the ENSO forecast models to predict the magnitude or rapid growth of the 1997/1998 El Niño, which occurred subsequent to a series of large MJO events in boreal winter/spring 1996/1997 (McPhaden, 1999; van

Oldenborgh, 2000; Barnston *et al.*, 2000), brought the problem to the fore. The question of the role of ISV in ENSO is part of a fundamental debate that revolves around the distinction between two views: ENSO seen as a quasi-cyclic mode of oscillation of the Pacific climate system (see Neelin *et al.* (1998) for a review), or as an initial value problem in which each El Niño is a largely independent event (Moore and Kleeman, 1999; Kessler, 2002b). In the first case, ISV is a source of noise that may contribute to irregularity of the cycle, but is not fundamental to it (Roulston and Neelin, 2000). In the second case an initiating perturbation external to ENSO itself is an essential element, and ISV could potentially provide it. (However, no one suggests that ISV *causes* the ENSO cycle itself, as is clear from the fact that coupled models without anything resembling the MJO develop fairly realistic ENSO cycles and statistics). Recently, theories have arisen that combine elements of these two viewpoints, arguing that the spatial characteristics of west Pacific westerlies associated with the MJO produce climate noise that is especially suited to influence a developing El Niño (Moore and Kleeman, 1999; Fedorov, 2002).

The occurrence of intraseasonal signatures in the ocean associated with El Niño was first noticed by Lukas *et al.* (1984), looking at central Pacific island sea levels, and others have followed using a variety of observed quantities (Enfield, 1987; McPhaden *et al.*, 1988; Kessler and McPhaden, 1995a, b; Kutsuwada and McPhaden, 2002; Zhang and Gottschalck, 2002). As described in the sections above, the ocean signatures include cooling under the strong winds and cloudiness of the west Pacific warm pool (e.g., Figure 6.3), and Kelvin-wave-mediated eastward advection and thermocline downwelling in the equatorial regions to the east.

There is no doubt that strong MJO activity is regularly seen during non-El Niño years, including its ocean signatures (Kessler *et al.*, 1995). Global interannual variability of the MJO is dominated by changes in the core region centered at 90°E, which are unrelated to ENSO (Hendon *et al.*, 1999; see also Figure 6.7, left-hand panel). Differences in MJO characteristics during El Niños have been noted, however. Several investigators have shown that MJO convection and surface zonal winds shift eastward during El Niño onset, from the far western Pacific to the eastern edge of the expanding warm pool (Gutzler, 1991; Fink and Speth, 1997; Hendon *et al.*, 1999; Kessler, 2001). Figure 6.7 shows that intraseasonal OLR in the warm pool region (150°E–180°) has large amplitude during El Niños that is not well correlated with the core intraseasonal OLR region over the Indian Ocean. During El Niños, ISV extends eastward (Figure 6.3), and its warm pool activity is in fact strongly correlated with the SOI ($r = -0.58$, see Figure 6.7, right-hand panel). Kessler (2001) showed that the eastward shift was not just incoherent ISV, which makes up perhaps half of the variance in this frequency band (Hendon *et al.*, 1999), but a systematic component of the organized MJO (note the large-scale events in Figure 6.3). The eastward shift is crucial to MJO/ENSO interaction because it can greatly increase the fetch of MJO winds over the Pacific (perhaps by a factor of two), thereby increasing the magnitude of the ocean signatures during those times.

The observed shift in the MJO envelope and its effect on the ocean was quantified by Zhang (2001) and Zhang and Gottschalck (2002), who suggested that an appropriate index could be based on the integral of MJO-filtered winds along

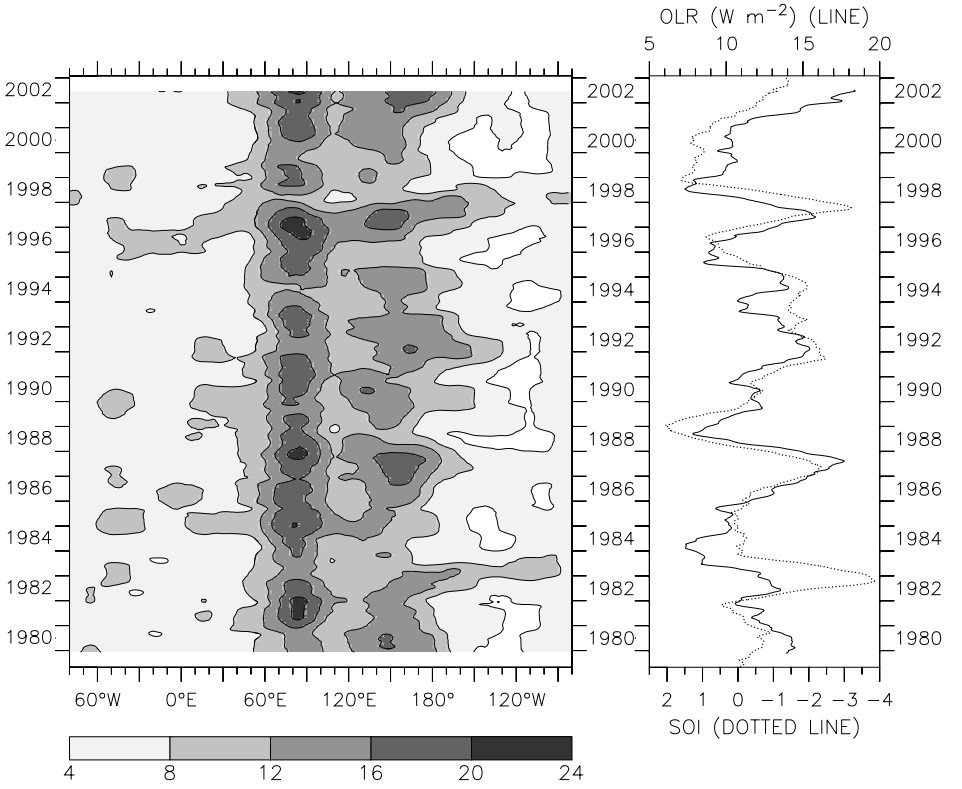

Figure 6.7. Interannual amplitude of intraseasonal outgoing long-wave radiation (OLR) (5°S–5°N) (W m^{-2}), defined as the one-year running standard deviation of intraseasonally-band-passed OLR. (*Left*) Amplitude in the global tropical strip, centered on the major region of variance at 100°E (the abscissa extends around the world, broken at the South American coast at 80°W). (*Right*) Time series of OLR amplitude averaged over the western Pacific (150°E–180°) (solid line, scale at top) in comparison with the SOI (dotted line, scale at bottom). Year ticks on each panel are at 1 January of each year, with year labels centered at mid-year. After Kessler (2001).

oceanic Kelvin wave characteristics. The index constructed in this way encompasses changes in the spatial pattern of the MJO as felt by ocean dynamics (though it does not consider changes in heat fluxes under the winds themselves). Zhang and Gottschalck (2002) used this technique to show that the MJO accounted for a significant fraction of interannual east Pacific SST variability, and that stronger El Niños (since 1980) were preceded by stronger MJOs. Although this work indicated a statistical relation between the intraseasonal and interannual frequencies, the rectifying mechanism still needs to be explained. If the MJO is simply an oscillation with zero mean, and the ocean feels this forcing linearly, there would be no interaction between frequencies. Several attempts have been made to elucidate such a mechanism.

One approach asks whether the occurrence of MJO events changes the background winds and heat fluxes over the Pacific. Ordinary statistical techniques used to extract MJO signatures from observations assume a linear separation between frequencies by band-pass filtering in some form to isolate the intraseasonal variance. The resulting zero mean time series are often taken to represent MJO anomalies with equal magnitude positive and negative phases. However, the realism of such representations has been questioned. If, for example, MJO events have systematically higher windspeed or westerly winds than the background, then anomalies defined to have zero mean will not adequately describe the effect on the ocean.

In the western Pacific where the background winds are often weak, the occurrence of large MJO wind oscillations implies stronger windspeed during *both* its easterly and westerly phases than in the absence of an MJO event, with correspondingly higher evaporation averaged over a cycle. Shinoda and Hendon (2002) showed that this process had an interannual modulation: MJOs represented in the US National Center for Environmental Prediction–National Center for Atmospheric Research (NCEP–NCAR) Reanalysis were more active over the warm pool during periods when the low-frequency winds were weak (probably because MJOs are restricted to the far western Pacific during La Niñas when strong trade winds extend westward), and thus on average the mean windspeed over a complete MJO cycle was enhanced by about $1\,\mathrm{m\,s^{-1}}$, with an averaged increased latent heat flux of about $23\,\mathrm{W\,m^{-2}}$. Zhang (1997) noted the difference in the effect of westerly anomalies on different backgrounds: during periods of mean easterlies (La Niña) a westerly wind burst represents a weakening of wind speed that will reduce latent heat fluxes, whereas on a westerly background, the same wind burst increases the wind speed and is a cooling term. Ocean models often use an *ad hoc* "gust factor" to represent disorganized small-scale wind speeds in the calculation of latent heat and mixing; this also tends to increase the wind speed produced by intraseasonal wind anomalies imposed in a model by limiting it on the low end. Kessler and Kleeman (2000) forced an ocean GCM with equal-amplitude easterly and westerly zonal wind anomalies (and a gust factor minimum of $4\,\mathrm{m\,s^{-1}}$) and found that the resulting higher windspeed produced SST cooling by about 0.6°C over an MJO cycle, compared to a climatological run. Although the gust factor influenced these results, SST cooling under stronger-than-climatology oscillating winds appears to be a robust feature of the MJO over the warm pool.

There are many other possibilities for rectifying interactions among the ocean responses to intraseasonal forcing, and these are just beginning to be explored. Waliser *et al.* (2003, 2004) forced an Indo-Pacific OGCM with realistic composite MJO and ISO anomalies and emphasized the potential for interaction between intraseasonal solar short-wave forcing and the ocean mixed layer. During the suppressed-convection phase of the MJO, positive short-wave anomalies occur in conjunction with low wind forcing; both of these act to stabilize and shoal the mixed layer and can produce SST warming. During the active-convection phase, the mixed layer deepens due to stronger winds and weaker solar heating; the result is that the cool anomaly is spread over a thicker layer and the negative SST change is not as

large as the positive change of the opposite phase, so the rectified signal is a warming. This appeared to explain their results in the maritime continent region where ocean dynamical processes play a little role.

Some have explicitly argued that MJO winds do not in fact have zero mean: the MJO composites of Waliser *et al.* (2003, 2004) showed that the westerly phase of MJO winds averaged about $0.5\,\mathrm{m\,s^{-1}}$ stronger than the easterly phase over the warm pool. Raymond (2001) presented a model of the MJO in which the convective systems were associated with westerly wind bursts without a corresponding easterly anomaly; when there is no MJO there are no bursts (see also Clarke (1994) for a discussion of the preference for westerly winds under equatorial convection). In such a model, the occurrence of MJOs changes the mean winds, thus the intraseasonal events have a low-frequency component. It is difficult to objectively define from observations what the background winds would be "without the MJO", and therefore what is the net signature of the MJO, especially because of their frequent occurrence during El Niño onset phases, when the low-frequency winds are turning westerly. Does the occurrence of a particular background foster more or stronger MJOs? Or, conversely, does the chance occurrence of more MJOs add up to a different background? It appears that the answer to both questions is "yes", and that makes definition of the total effect of intraseasonal forcing a fuzzy concept. The best answer that can be given today is that the passage of an MJO across a large region of the west Pacific appears to be more likely during El Niño onset, when warming SST is spreading eastward, and the result of this passage is an increase in both westerly winds and wind speed over a wide zonal extent. We can now ask: how might these forcing changes interact with the coupled dynamics of the ENSO cycle?

One of the earliest attempts to quantify the effect of a short-term westerly event on the Pacific was by Latif *et al.* (1988). They forced a coupled GCM with a single, 30-day "westerly wind burst", with $10\,\mathrm{m\,s^{-1}}$ winds extending over 10°S–10°N, from the western boundary to 180°, after the model had achieved a stable climatology. Following the imposed burst, the coupled model was allowed to evolve freely. While the response of an uncoupled ocean model to such an event is short-lived, the coupled system developed long-term changes. An eastward shift of the area of warmest water to about 160°W led to an eastward shift of convection. The model atmosphere responded with persistent westerlies blowing into the convection, in a self-sustaining feedback which maintained the eastward-shifted SST and convection for more than a year. The Latif *et al.* (1988) experiment suggested that the coupled system is capable of rectifying short-term wind anomalies into a low-frequency change because the rapid response of the atmosphere to SST changes can reinforce the ocean anomalies before they have dissipated.

Around the same time, an experiment with a simple coupled model came to the opposite conclusion. Zebiak (1989) added intraseasonal noise to the model-generated zonal wind field in the Zebiak and Cane (1987; hereafter ZC) coupled model and found little impact on the evolution of the modelled ENSO cycle. The imposed ISV produced only a spread to the forecasts, not a systematic change in ENSO amplitude. Moore and Kleeman (2001) noted the insensitivity of the ZC model to perturbations in the western Pacific, and attributed it to the way

atmospheric latent heating (that spurs the growth of convection) is treated over the warm pool where in reality small SST anomalies can produce a strong flowering of convection. This process is inhibited in the ZC model, and is a major difference from the coupled GCM of Latif *et al.* (1988). Another difference is that SST anomalies in ZC are closely tied to thermocline depth fluctuations, which is appropriate in the central and eastern Pacific but much less so in the west, where the background thermocline is very deep and surface fluxes dominate (McPhaden, 2002; see Section 6.2.2). Although the ZC model has shown notable success in forecasting the ENSO cycle, it is probably the wrong tool to investigate the effects of ISV.

A simple model of MJO rectification under zero mean winds was proposed by Kessler *et al.* (1995), based on a similar idea as Latif *et al.* (1988) discussed above: the atmosphere responds within days to SST changes by shifting the location of convection and associated westerlies, but the ocean's response to winds is lagged because it integrates the forcing. The rapid atmospheric shift is seen in Figure 6.3 as the intraseasonal winds following the maximum SST gradient eastward. Kessler *et al.* (1995) modeled this in highly idealized form by assuming that organized intraseasonal winds occur only over the warm pool, and that the wind fetch responds instantly to changes in the warm pool zonal width. Westerly winds generate Kelvin wave currents that advect the east edge of the warm pool eastward, and easterly winds do the opposite. As the warm pool width changes, so does the region of convection and the fetch of the oscillating winds: westerly winds increase the width and easterly winds decrease it. Thus, westerly winds increase their own fetch and easterlies decrease it, thus the ocean feels the eastward advection more strongly. The net effect of oscillating intraseasonal winds is to push the warm pool slowly eastward; in the idealized Kessler *et al.* (1995) model this was found to resemble the stepwise eastward expansion of warm SST seen during El Niños. The fact that the east edge of the warm pool is also a salinity front contributes an additional positive pressure gradient term that can enhance the eastward advection (Lengaigne *et al.,* 2002).

Kessler and Kleeman (2000) explored the consequences of the net latent heat cooling produced by the high windspeeds due to oscillating winds on a weak background. In an intermediate coupled model, slightly cool SST (presumed to have been generated by a series of MJOs) was imposed on the Pacific west of about 160°E, during the period just as the 1997/1998 El Niño was beginning. In fact, observations showed cooling of the far west Pacific at this time (Figure 6.3, see also McPhaden, 1999). Hindcasts of the 1997/1998 event were made with and without the imposed cooling. The control run produced a weak El Niño, typical of the forecasts that were made by many models before the event. The imposed-cooling run developed persistent westerlies blowing out of the cool western region; these increased the El Niño SST anomalies by about 30%, which improved the realism of the hindcast. They suggested that the MJO can thus act constructively on ENSO as a stochastic amplifier, and that the weather-like unpredictable nature of MJOs may make forecasting the amplitude of an oncoming El Niño event more difficult than predicting the occurrence of the event itself.

A different sort of rectifying process has been proposed to explain the perplexing discrepancy between the 40–50-day MJO signals observed in the atmosphere

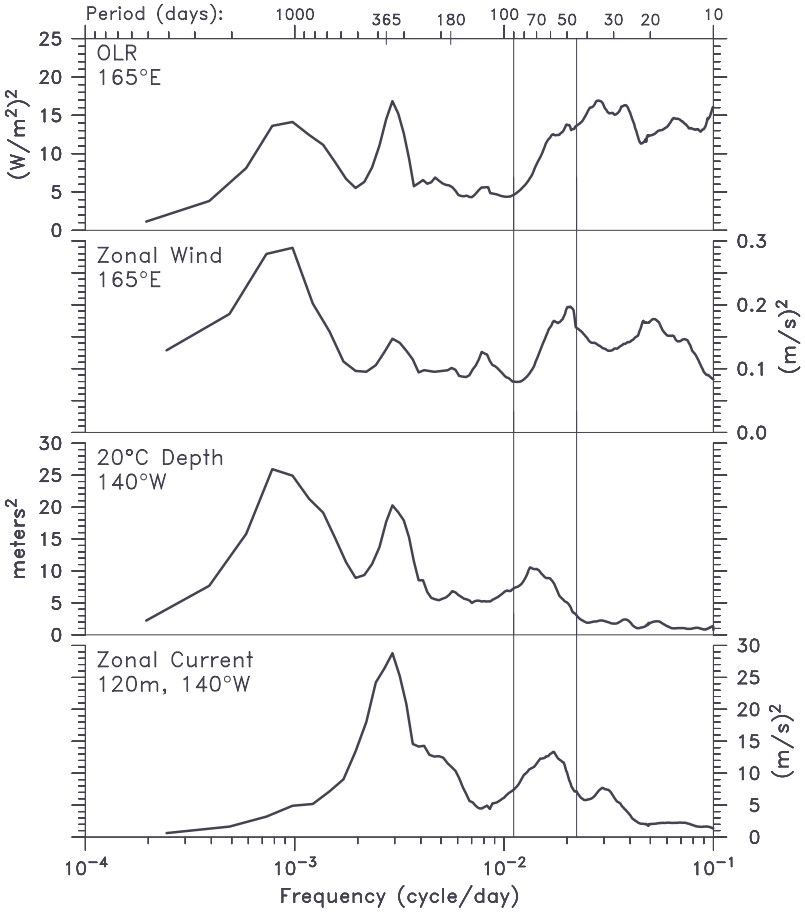

Figure 6.8. Variance-preserving spectra of OLR at 165°E, zonal wind at 165°E, 20°C depth at 140°W, and EUC speed at 140°W, 120°m depth, all at the equator. Each variable has a separate scale as indicated. The spectra are calculated for the 10-year period April 1983–April 1993 for all quantities except zonal wind, for which only the 7-years data, July 1986–July 1993, were available.
After Kessler *et al.* (1995).

(Madden and Julian, 1994) and the 60–70-day periods that dominate the ocean Kelvin wave response (Enfield, 1987; Kessler *et al.*, 1995, among others). Figure 6.8 shows variance-preserving spectra of two atmospheric quantities at 165°E (OLR, and zonal winds measured by the TAO buoy there), and two ocean quantities at 140°W (thermocline depth and zonal current at undercurrent level), which experience little local intraseasonal forcing, but strongly feel ISV through Kelvin wave propagation from the western Pacific. The intraseasonal variance of both the atmospheric quantities falls off sharply at periods longer than about 55 days, while the corresponding peak for both ocean quantities is clearly shifted to a lower frequency.

As noted above, the Kelvin wave amplitude east of a patch of oscillating zonal winds depends on the integral of the forcing along the wave characteristic. For steady winds, this is proportional to the time it takes the Kelvin wave to cross the patch, L/c, where L is the patch width and c is the wave speed (about $2.5\,\mathrm{m\,s^{-1}}$), but for oscillating winds the response is smaller because the winds may change sign while the wave is still traversing the patch. As the frequency of the wind increases to the point where the Kelvin wave crosses the patch in one period ($P = L/c$), the wave feels an equal amount of easterlies and westerlies, so the forcing integral cancels exactly and the response east of the patch falls to zero. Kessler *et al.* (1995) showed that for a 5,000 km width patch, there is a rapid fall-off in Kelvin wave amplitude between roughly 100-day and 30-day period oscillations, and suggested that this would account for the preference for lower intraseasonal frequencies in the ocean east of the warm pool (Figure 6.8). Hendon *et al.* (1998) improved on this crude fixed-patch model by considering the more realistic eastward propagation of MJO forcing over the warm pool, which moves at speeds similar to the Kelvin wave (Hendon and Salby, 1994). When the MJO speed equals the Kelvin wave speed, the forcing is resonant and the Kelvin amplitude is the same as for steady winds; in other cases it is less. For a realistic MJO wind, this maximum occurs at periods of about 70 days, and falls off very rapidly at higher frequencies. They conclude that the observed frequency offset between atmosphere and ocean is due to these linear Kelvin wave dynamics as a consequence of the spatial and temporal characteristics of the MJO winds.

6.6 ISV IN THE INDIAN OCEAN

The Indian Ocean is much more poorly observed than the Pacific; as a result much of the diagnosis has been done in models, often without adequate observational confirmation. Many hypotheses have been raised in model studies that cannot be fully substantiated and remain speculative. This situation is slowly being rectified through large-scale sampling (e.g., the Argo array of profiling floats, Gould *et al.* (2004)), and through regional programs (e.g., JASMINE, see Webster *et al.*, 2002). Schott and McCreary (2001) give a comprehensive review of the present state of knowledge of Indian Ocean circulation, focusing on the dynamics of the large-scale and low-frequency signals. Another useful overview is the textbook of Tomczak and Godfrey (1994), while Swallow (1983) reviews *in situ* observations of Indian Ocean eddies.

6.6.1 Differences between the Indian and Pacific Ocean warm pools and their consequences

The physical processes by which the Indian Ocean responds to intraseasonal forcing are the same as those of the Pacific, but differences in the background conditions have a large influence on the oceanic consequences. The shape of the Indian Ocean basin has an important effect because it is closed in the northern subtropics. In the Pacific (or Atlantic) equatorial Kelvin waves reflect along the eastern boundary to

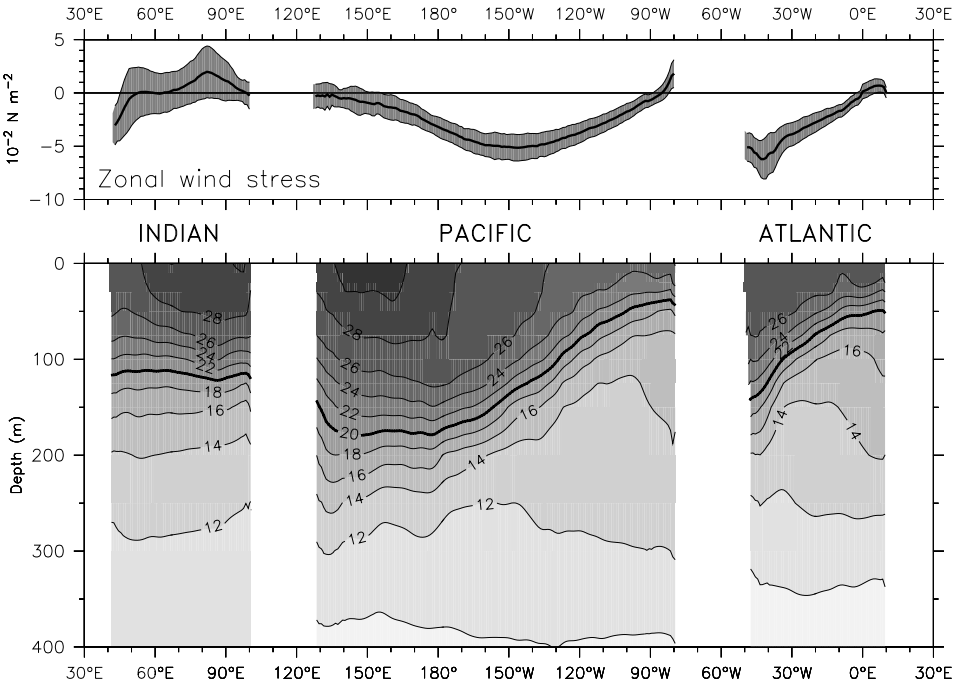

Figure 6.9. Mean zonal wind stress (*top*) and upper ocean temperature (*bottom*) along the equator. The winds are from the ERS scatterometer during 1992–2000, averaged over 5°S–5°N. The heavy line shows the mean, and the gray shading around it shows the standard deviation of the annual cycle. The ocean temperatures are from the Levitus (1994) *World Ocean Atlas*, with a contour interval of 2°C, and a supplemental contour at 29°C.

coastal signals that propagate poleward; as a result intraseasonal wind forcing becomes "lost" to the tropics in those basins. In the Indian Ocean, in contrast, coastal waves are directed into the Bay of Bengal (and from the Bay around the southern tip of India into the Arabian Sea), providing an important source of remote forcing to the off-equatorial tropics originating in equatorial winds (Potemra *et al.*, 1991; McCreary *et al.*, 1993; Schott *et al.*, 1994; Eigenheer and Quadfasel, 2000; Somayajulu *et al.*, 2003; Yu, 2003; Waliser *et al.*, 2004).

The fact that the climatological semi-annual wind forcing is much stronger than the mean winds in the Indian Ocean distinguishes it from the other basins that have permanent equatorial easterlies and thus a permanent zonally sloping thermocline and EUC, with their accompanying warm pool in the west and cold tongue due to upwelling in the east. The shallow east Pacific thermocline allows remotely forced thermocline depth changes to quickly and easily affect SST and thereby provide the potential for coupled interaction. Figure 6.9 shows the mean zonal thermocline slope associated with the mean easterlies in the Pacific and Atlantic, and the contrasting flat, deep thermocline of the Indian Ocean. Because of this profound difference in structure, the fluent communication between ocean dynamical processes and the

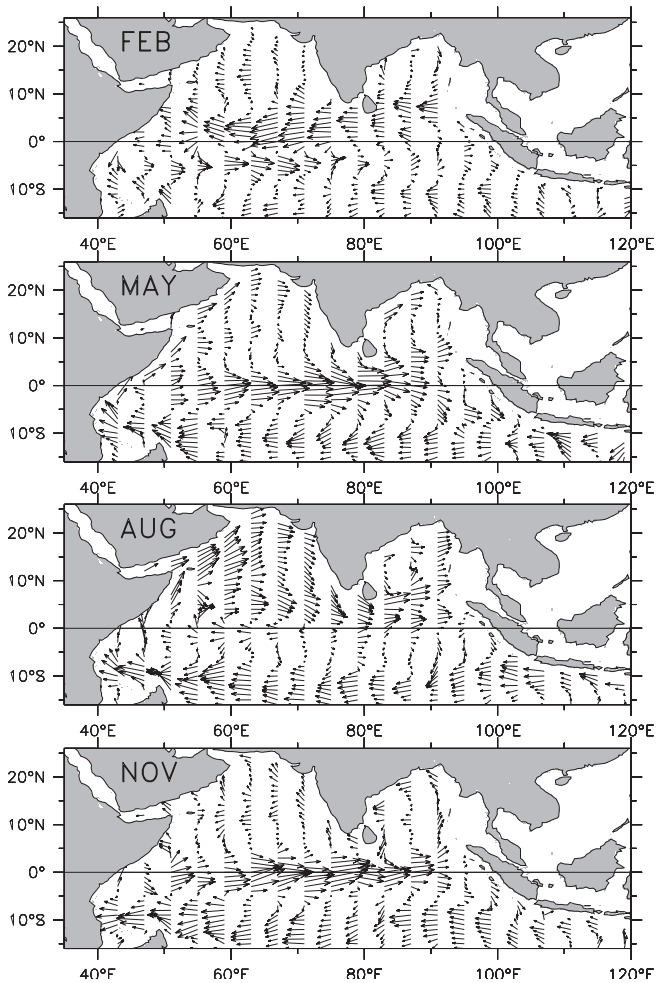

Figure 6.10. Seasonal cycle of Indian Ocean surface currents from historical ship-drift data (Mariano *et al.*, 1995). North of about 8°S the annual and semi-annual variation of most currents is much larger than the mean. The Wyrtki Jets are the equatorially-trapped eastward currents during May and November. The dramatic seasonal reversals of circulation in the Arabian Sea, the Bay of Bengal, and along the African Coast (Somali Current) are also evident.

atmosphere as occurs in the Pacific (Sections 6.4 and 6.5) is much more difficult to accomplish in the equatorial Indian Ocean. (However, an interannual "Indian Ocean Zonal Mode" has been proposed that depends on such changes in the narrow upwelling region close to the coast of Java; see Webster *et al.* (1999), Saji *et al.* (1999), Murtugudde *et al.* (2000), and Annamalai *et al.* (2003).)

The semi-annual equatorial zonal winds spin up eastward Yoshida Jet-like features in May and November (Wyrtki Jets; Figure 6.10) in response to westerly

maxima during the monsoon transition seasons (Wyrtki, 1973; Reverdin, 1987; Han *et al.*, 1999). Although the climatological picture suggests two well-defined jets, observational (Reppin *et al.*, 1999) and modeling studies (Masson *et al.,* 2003) show that each semi-annual jet is broken up into oscillations with timescales of a month or less. As the zonal pressure gradient adjusts to the monsoon transition winds (see Section 6.3), semi-annual Kelvin waves are generated that contribute to the seasonally-reversing boundary currents in the Bay of Bengal (see references above), and by interacting with the locally-generated flow field there, contribute to its rich intraseasonal eddy field (Vinayachandran and Yamagata, 1998). This source of semi-annual remote forcing adds to the local intraseasonal forcing in boreal summer (Waliser *et al.*, 2004) to produce variability throughout the year, which may be one reason why the Bay of Bengal eddies do not appear to be strongly seasonally modulated (Somayajulu *et al.*, 2003).

In the central equatorial Pacific, meridional winds are weak compared to zonal winds, and the zonal winds are relatively uniform in latitude within 5°N–5°S. Thus the meridional circulation there is largely symmetric with a nodal point at the equator, and cross-equatorial oceanic heat transport occurs principally through mixing and small-scale processes (Blanke and Raynaud, 1997). In the Indian Ocean, by contrast, meridional winds are strong and seasonally reversing, and zonal winds are antisymmetric across the equator. This allows a significant mid-basin cross-equatorial (mean southward) Ekman mass transport (Miyama *et al.*, 2003) that balances the large cross-equatorial western boundary current mass transport driven by monsoon winds (the Somali Current, see Section 6.7.3); such a circulation has no counterpart in the other oceans. Similarly, in the west Pacific warm pool, the annual cycle of SST is damped by the tendency for convective cloudiness to increase with surface temperature (Ramanathan and Collins, 1991). In the North Indian Ocean, by contrast, the short-wave heat flux has a strong annual cycle because convection is absent during boreal spring. However, the annual cycle of SST there (east of the Somali Current region) is also small (Murtugudde and Busalacchi, 1999), comparable to that of the Pacific warm pool. Loschnigg and Webster (2000) suggested that this requires a seasonally-reversing oceanic cross-equatorial heat transport of the order of ± 1.5 PW, northward in winter and southward in summer, to maintain the SST (Figure 6.11). In their model, this transport was produced by a combination of western boundary and interior Ekman flows, driven by monsoon winds. It was strongly intraseasonally modulated. On the other hand, Waliser *et al.* (2004) found a similar seasonal but much smaller intraseasonal cross-equatorial transport oscillation in their ocean GCM and commented that the simplicity of the Loschnigg and Webster (2000) 2.5-layer ocean model might have led to an overestimate by neglecting the complex baroclinic variations.

The extreme rainfall and riverine input to the Bay of Bengal give it a surface salinity at least 1 psu fresher than the west Pacific warm pool (Bhat *et al.*, 2001) and low surface salinity extends across the equator in the eastern basin (Sprintall and Tomczak, 1992; Han *et al.*, 2001b). The resulting barrier layer is much stronger than in the Pacific warm pool (Section 6.2), especially in the western Bay (Shetye *et al.,*

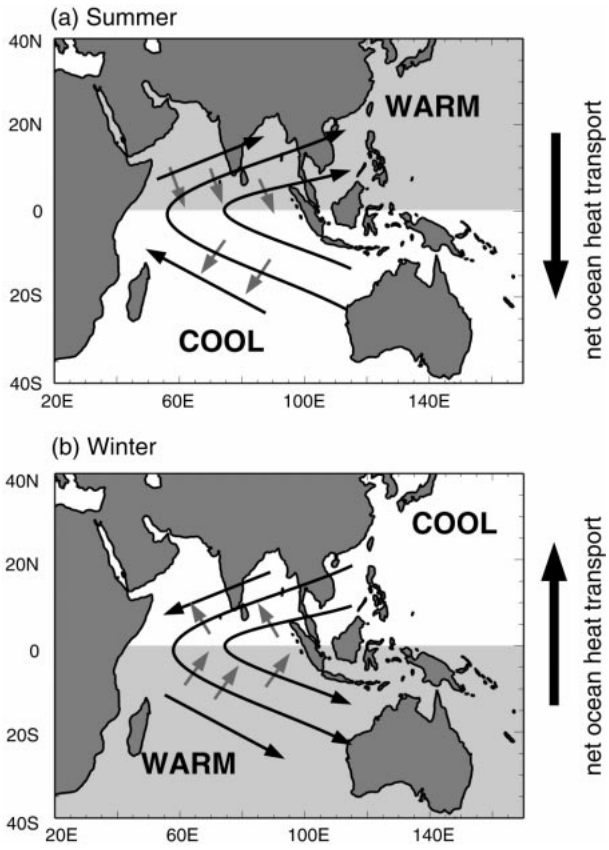

Figure 6.11. A regulatory model of the annual cycle of the Indian Ocean monsoon system depicted for (a) summer (June–September) and (b) winter (December–February). Curved black arrows denote the wind forced by the large-scale differential heating denoted by "warm" and "cool". The small gray arrows are the Ekman transport forced by the winds. The large vertical black arrows to the right show the net ocean heat transport that reverses between summer and winter. The net effect of the combined wind-forced ocean circulation is to transport heat to the winter hemisphere, thus modulating the SST differences between the hemispheres.
After Loschnigg and Webster (2000).

1996), and enlarges down to the equator most prominently in boreal fall (Masson *et al.*, 2002). As in the west Pacific warm pool, the barrier layer enhances the surface speed of the boreal fall Wyrtki Jet by trapping wind momentum in a thin surface layer (Section 6.2); Han *et al.* (1999) estimated this effect at $0.3\,\mathrm{m\,s^{-1}}$. In a model forced by observed precipitation, Masson *et al.* (2002, 2003) further suggested that advection of a subsurface salinity maximum by the Jet contributes to the intensification of the barrier layer in the eastern equatorial Indian Ocean.

The Indonesian Throughflow (ITF) exerts a fundamental control on the

Indo-Pacific warm pool; coupled model experiments suggest that it results in a warming of the Indian Ocean while cooling the Pacific and shifting the warm pool to the west (Schneider, 1998). Therefore, factors that influence ITF mass and property transport variability are of great interest. Velocities through the narrow ITF outflow straits can be significantly affected by Kelvin waves forced by equatorial winds and propagating along the Java coast at intraseasonal and semi-annual frequencies (Qiu *et al.,* 1999; Potemra *et al*., 2002; Waliser *et al*., 2003). These waves modulate sea level on the Indian Ocean ends of the straits and therefore change the along-strait pressure gradients; there may also be property effects due to changing the baroclinic structure of the outflows (Potemra *et al*., 2003; Sprintall *et al*., 2003). Qiu *et al*. (1999). Durland and Qiu (2003) also showed that intraseasonal Kelvin waves enter the Indonesian Seas at the Lombok Strait (a major outflow into the Indian Ocean) and modulate sea level in the Makassar Strait; this means that the straits further east (Timor and Omboi) are much less affected by Indian Ocean equatorial ISV. Although the intraseasonal equatorial forcing is a major influence on the velocity at Lombok, it is not yet clear whether this variability has a significant effect on the properties on the Indian Ocean side that would contribute to subsequent variability (Sprintall *et al*., 2003).

It is worth noting that Qiu *et al*. (1999) also identified an ISO in the Celebes Sea that is unrelated to TISO winds. Their model results suggested that as the Mindanao Current retroflects into the Pacific at about 4°N, it sheds eddies into the Celebes Sea that closely match the gravest Rossby mode of this semi-enclosed basin, leading to resonance.

6.6.2 26-day oscillations in the western equatorial Indian Ocean

Meridional current oscillations concentrated on a narrow band of periods near 26 days were first observed by moorings in the western equatorial Indian Ocean in 1979–1980 (Luyten and Roemmich, 1982). There was very little zonal current signal in this band. Subsequently, similar oscillations were found in drifter tracks just north of the equator (Reverdin and Luyten, 1986), which raised the possibility that these were Tropical Instability Waves (TIW; see Section 6.7.2) similar to those in the Pacific and Atlantic. However, the close association of TIW with zonal current shear was not seen in the Indian Ocean. Models forced with smoothly-varying monthly winds were able to reproduce the 26-day waves, and showed that their dispersion properties (wavelength, westward phase propagation, and eastward group velocity) were consistent with Yanai wave kinematics (Kindle and Thompson, 1989). Tsai *et al*. (1992) used satellite SST to examine the spatial and temporal properties of the oscillations in this frequency band. These data confirmed the 26-day period, and its characteristics were consistent with westward-phase-propagating Yanai waves. The oscillations were found from 52°E to 60°E, about 1,000 km east of the coast. There have been two explanations proposed for the generation of these waves, which are apparently not forced by anything in the local winds. Moore and McCreary (1990) suggested that a periodic wind stress along the slanting western boundary could produce such Yanai waves propagating

into the interior. However, several models (e.g., Kindle and Thompson, 1989) have produced 26-day Yanai waves when forced with climatological monthly winds alone. In these models, the waves were generated as an instability of the Somali Current system southern gyre (Schott and McCreary, 2001), a completely different mechanism than that which produces the TIW. It is not known why there is a preference for the apparently robust 26-day period.

6.6.3 Recent models of wind-forced ISV in the Indian Ocean

Using the detailed new satellite wind and SST products, modelers have begun to attempt simulations of Indian Ocean ISV forced with realistic winds and compared to realistic SSTs. Although many of the processes found are similar to those previously diagnosed in the Pacific, several studies have tried to disentangle the oceanic ISV due to TISO wind forcing vs. that due to internal instabilities.

Han *et al.* (2001a) noted the occurrence of two distinct peaks in simulated zonal currents in the central and eastern Indian Ocean, at 40–60 days and at 90 days. Comparing model runs with and without the intraseasonal winds showed that the 40–60-day signals were a predominantly linear ocean response to direct wind forcing. In the central and eastern basin, much of this variability was associated with organized, eastward-propagating MJO winds. The 90-day current peak, however, was significantly different from the forced linear solution. Part of the difference could be explained by a mechanism similar to that found in the Pacific by Kessler *et al.* (1995) and Hendon *et al.* (1998), in which the ratio between the period of the forcing and the time it takes a wave to cross the wind patch can lead to lower frequencies being preferentially felt by the ocean (see Section 6.5). However, in the Indian Ocean, reflected Rossby waves can be an additional influence because the distance from the region of strong intraseasonal winds and the eastern boundary is much shorter than it is in the Pacific. Han *et al.* (2001a) showed that a second baroclinic mode equatorial Kelvin/reflected Rossby wave is nearly resonant in the Indian basin when forced with 90-day period winds (also see Jensen, 1993), and thereby enhances the eastern ocean response at that period.

Sengupta *et al.* (2001) compared the results of an OGCM forced with full wind variability and with filtered seasonal cycle winds. Even when forced with smooth seasonal cycle winds, their model developed intraseasonal current variability in the western boundary region (see Section 6.7.3) and also south of Sri Lanka in the central basin, similar to observations (e.g., Figure 6.12). Tracing individual Kelvin waves and their Rossby reflections showed that the Sri Lanka ISV in this model was due to intraseasonal vortices generated when the eastern boundary Rossby reflections of the semi-annual Wyrtki Jet Kelvin waves meet the background eastward South Monsoon Current (Vinayachandran and Yamagata, 1998; Schott and McCreary, 2001). The fact that the Sri Lanka ISV in a complete-forcing run agreed in phase with observed velocities strongly suggested that despite the development of instabilities, these signals were predictable, and thus at least quasi-linear, responses to the winds.

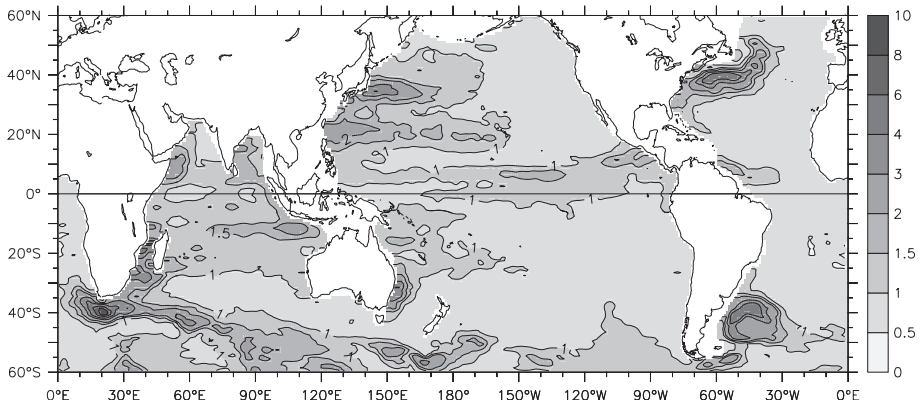

Figure 6.12. RMS of band-passed (35–85-day half power) sea level from the TOPEX/Poseidon satellite altimeter, for data during January 1992–July 2003. Dark shading indicates high sea level RMS, with a stretched contour interval (values indicated in the scale on the right).

6.7 OTHER INTRINSIC OCEANIC ISV

6.7.1 Global ISV

There is such a large variety of intrinsic ISV in the oceans, caused by many processes other than intraseasonal atmospheric forcing, that a review of the entire subject is well beyond the scope of this chapter. In addition, much of this variability is not germane to the principal thrust of this book. We will therefore focus on the most common signals that are likely to be intermingled with wind-forced ISV in the tropics, and that could therefore cause confusion in the interpretation of ocean observations connected with TISO. Other regional ISV signals will be discussed only briefly.

As an index of the occurrence of ISV in the global ocean, Figure 6.12 shows the RMS of intraseasonally band-passed sea level (sea surface height (SSH)) from the TOPEX/Poseidon altimeter (Fu *et al.*, 1994). It shows distinct regions with strong SSH ISV in many parts of the World Ocean; most of these are not associated with the tropical ISOs that are the principal subject of this book. Note that the equatorial region discussed above does not appear as a strong maximum of SSH ISV. That principally reflects the fact that small pressure gradients are more effective at driving currents near the equator because of the small value of the Coriolis parameter. Many investigators have studied altimetric SSH as an index of eddy variability, sometimes using it to estimate eddy kinetic energy through a geostrophic assumption which emphasizes the tropics (Stammer, 1997). Also note that the TOPEX altimeter does not sample small-scale very-near-coast signals very well, which is probably why the coastal Kelvin waves mentioned in Section 6.4 do not appear in Figure 6.12.

6.7.2 Non-TISO-forced ISV in the tropical Indo-Pacific

Two important intraseasonal phenomena that are not forced by TISO are observed in the tropical Pacific: the Tehuantepec and Papagayo eddies, which produce the

bands of high ISV extending south-west from Central America in Figure 6.12, and the tropical instability waves, which are seen as the strip of SSH variability along 5°N. Although these two signals appear continuous in Figure 6.12, they are entirely separate phenomena (Giese *et al.*, 1994).

Central American eddies

The Tehuantepec eddies are generated by episodic winds blowing through the mountain pass at the Isthmus of Tehuantepec in southern Mexico (Chelton *et al.*, 2000b; Kessler, 2002a). High pressure behind winter cold fronts transitting North America causes a cross-mountain pressure gradient that funnels an intense wind jet through the pass and over the Pacific, on timescales of a few days (Hurd, 1929; Roden, 1961; Chelton *et al.,* 2000a). These winds produce locally strong mixing and SST fluctuations (Trasviña, 1995), and also generate a series of typically three to five anticyclonic (warm-core) eddies each winter that propagate westward approximately as free Rossby waves (Giese *et al.*, 1994), leading to the strip of high SSH variance in Figure 6.12. Individual eddies can be tracked in SSH along 11°N on occasion as far west as the dateline (Perigaud, 1990; Giese *et al.*, 1994; see also Figure 6.13). Ocean color is a useful technique for remotely sensing these eddies because their SST signal may be small, but the associated plankton blooms can still be evident (McClain *et al.*, 2002). While the forcing occurs on a timescale much shorter than intraseasonal, the fact that the wind events occur episodically several times each winter results in the apparent intraseasonal timescale. The observed preference for anticyclonic rotation was explained by McCreary *et al.* (1989): although eddies of both signs are generated by the wind jet (downwelling under the negative curl region on the right flank of the jet axis, upwelling on the left flank to the east), the high winds quickly mix away the upwelled thermocline of the cyclonic eddy.

Winds blowing through the lowlands of Nicaragua (known as Papagayo winds) are less variable than those through Tehuantepec, and not apparently associated with mid-latitude cold fronts, though they are still stronger in winter (Müller-Karger and Fuentes-Yaco, 2000; Chelton *et al.*, 2000a, 2000b). A different explanation for the eddies west of Nicaragua (seen as the southern strip of high intraseasonal variance west of Central America in Figure 6.12) was proposed by Hansen and Maul (1991), who estimated a propagation speed greater than that of free Rossby waves and diagnosed the eddies as strongly non-linear and similar to Gulf Stream rings. They suggested that the Papagayo eddies, which are also anticyclonic, could be due entirely to ocean dynamics, without any influence of the mountain-gap winds. Instead they point to conservation of potential vorticity as the North Equatorial Countercurrent (NECC), which is strongest in boreal winter, turns sharply northward when it meets the coast. They proposed that the anticyclonic relative vorticity gained in the northward flow results in eddy shedding. This hypothesis has been questioned (Giese *et al.*, 1994), and the possible difference in generation mechanism between the Papagayo and Tehuantepec eddies has not been resolved. Eddies are also seen west of a third wind jet through the lowlands of Panama

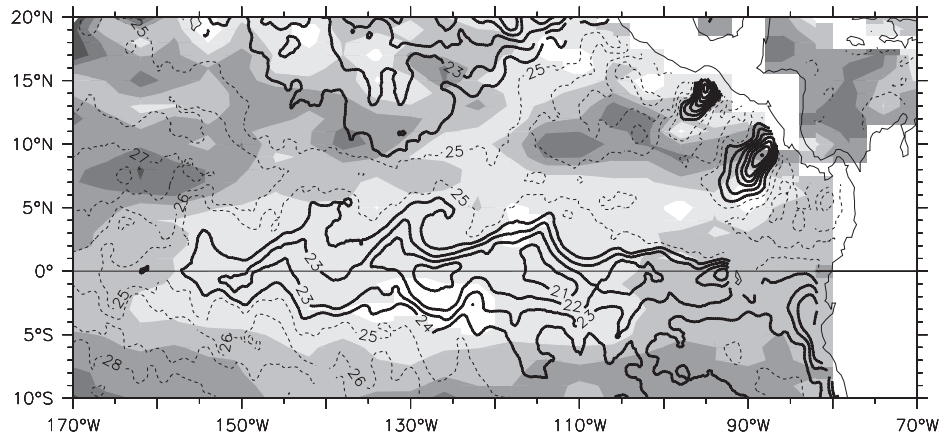

Figure 6.13. Example of the sea surface topography (shading) and temperature (contours) observed by satellite during January 2000, illustrating the signatures of the Central American eddies and of the tropical instability waves (Section 6.7.2). The eddies are visible as the four dark patches lined up along 8°N–12°N; these are warm-core (anticyclonic) vortices produced by episodic mountain-gap winds through the Central American Cordillera. They propagate west with a speed of about 15 cm s^{-1} (400 km month^{-1}). The direct SST effects of the winds are seen as the packed dark (cool) contours that indicate the location of the strongest winds at Tehuantepec and Papagayo. The dark SST contours along the equator show the cold tongue (a SST greater than 25°C is indicated by dashed contours). The cusps along the tight SST gradient on the north side of the tongue are the signature of tropical instability waves. These waves propagate west with a speed of about 1,000 km month^{-1}.

(Müller-Karger and Fuentes-Yaco, 2000; note the third, weaker strip of ISV in Figure 6.12), but these have been studied even less.

The offshore passage of these eddies, however generated, was documented by Giese *et al.* (1994) using TOPEX altimetry, and by Hansen and Maul (1991) using surface drifter tracks. Confusingly, the Tehuantepec eddies appear to first move south-west and then follow the same track along 11°N as the Papagayo eddies westward from Central America (Giese *et al.*, 1994; see also Figure 6.12); it is not known why this behavior occurs. Their speed along 11°N is about 17 cm s^{-1}, which is close to the theoretical first baroclinic mode Rossby wave speed at that latitude. The spatial scale of the eddies is a few hundred kilometers, and they tend to be zonally-elongated (Giese *et al.*, 1994; see also Figure 6.13). It is unlikely that the offshore eddies would interact with the ocean variability due to TISO forcing, because they are far enough from the equator to be well poleward of the Kelvin wave influenced region, and they die out east of the warm pool where the TISO signals have a wider meridional span. However, near the coast an interaction is possible, because TISO-forced equatorial Kelvin waves (Section 6.4) produce strong intraseasonal velocity and thermocline depth variability as their reflection leaves poleward-propagating coastal waves (note that the TISO Kelvin waves also display a preference for down-welling). An apparent coincidence between the arrival of TISO-origin Kelvin waves

and the shedding of offshore-propagating eddies led to speculation that perhaps some of the Central American eddies were in fact triggered or modulated by TISO (B. Kessler, pers. commun., 1998), though the mechanism is unclear. Linear wave theory does not encompass the dynamics of coastal Kelvin wave propagation when a zonally-oriented coast is part of the picture, as occurs at the Isthmus of Tehuantepec; this problem has been glossed over (see the appendix to Kessler *et al.*, 2003).

Tropical Instability Waves

TIW were recognized as soon as satellites began observing SST, as the cusps in the sharp front near 2°N between the east Pacific cold tongue and warmer water along the North Equatorial Countercurrent (Legeckis, 1977). They are particularly obvious in their SST patterns (Chelton *et al.*, 2000c; Contreras, 2002), distorting the front into 1,000–1,500 km long cusp shapes (rounded to the south, pointed to the north; Figure 6.13). Since then, they have also been observed in satellite altimetry (Musman, 1989; Weidman *et al.*, 1999), surface drifter tracks (Hansen and Paul, 1984; Flament *et al.*, 1996; Baturin and Niiler, 1997), satellite ocean color (McClain *et al.,* 2002), and moored temperature and velocity time series (Halpern *et al.*, 1988; McPhaden, 1996), and are a robust and commonly-observed aspect of the eastern tropical Pacific (and Atlantic). In addition they are a ubiquitous feature of ocean GCMs (Cox, 1980; Philander *et al.*, 1986; Kessler *et al.*, 1998; Masina and Philander, 1999). With very large meridional velocity fluctuations, of the order of $\pm 50\,\mathrm{cm\,s^{-1}}$, TIW are a substantial source of noise that pose difficult aliasing problems in typically sparse ocean observations, even to sample the mean (Johnson *et al.*, 2001). TIW arise in the far eastern Pacific and propagate west with speeds of about $30–60\,\mathrm{cm\,s^{-1}}$ (about 10° longitude per month), weakening west of about 150°W. It has not been clear how far west they penetrate, since as the SST front weakens to the west their SST signature that is easiest to observe dies away. Their frequency spans 20–35 days. A feature that has caused confusion is the apparent difference in frequency depending on the quantity being observed, with SST (whose signature is seen in the SST front near 2°N) showing a dominant period of about 25 days (Legeckis, 1977), whereas altimetric sea level (seen near 4°–6°N) appears to have a period near 35 days (Chelton *et al.*, 2003), and equatorial velocity a period near 21 days (Halpern *et al.*, 1988). These discrepancies may be the result of a fairly broadband instability shedding quasi-linear Yanai waves preferentially at certain frequencies (e.g., Weisberg *et al.*, 1979). Although the TIWs were first identified north of the equator, and their strongest signals continue to be found there, recent work has shown the existence of TIWs to the south (Chelton *et al.*, 2000c).

The principal mechanism producing the TIW is thought to be barotropic (shear) instability as first explained by Philander (1976, 1978). Since it is very difficult to diagnose energetics from sparse ocean observations, most of this work has been done in numerical models of various types (however, see Luther and Johnson (1990) and Qiao and Weisberg (1998) for observational analyses). The meridional shear in the equatorial Pacific is complex, with several strong oppositely-directed zonal currents in close proximity (Luther and Johnson, 1990; Johnson *et al.*, 2002), and there has

been an evolution in thinking about this problem. The original Philander analysis concluded that the relevant shear was near 4°N between the westward SEC and the eastward NECC. More recent work points to the shear close to the equator between the SEC and the EUC; in addition the possibility of baroclinic instabilities associated either with the spreading isotherms around the EUC or with the sharp temperature front appears to be important as well (Yu *et al.*, 1995; Masina *et al.*, 1999). The sources of energy conversion driving the TIW remains an active area of research, and it is likely that different mechanisms come into play at different latitudes, perhaps explaining the multiple frequency structure seen. However, the fact that ocean GCMs of diverse types easily generate TIWs, whether forced with realistic or highly simplified winds, suggests that near-equatorial zonal shear is the dominant factor. The contribution to the variability by free-wave propagation out of the instability growth region is another current area of research. It has not been clear exactly how far east the TIWs begin, nor what is the initiating perturbation. All three currents involved are weaker in the far east (Johnson *et al.*, 2002; Lagerloef *et al.*, 1999) (but note that the Costa Rica Dome circulation may provide more shear east of 95°W; see Kessler, 2002a).

Because the TIWs depend on the background conditions, which vary seasonally and interannually, their low-frequency modulation is expected. The entire upper-equatorial circulation quickens when the winds are strongest in June–December: the westward SEC and eastward NECC are largest in boreal fall, as is equatorial upwelling (Kessler *et al.*, 1998). These conditions produce both the strongest meridional shears and sharpest temperature front, so it is not surprising to find that the TIWs appear in May or June and persist through the following February–March. Similarly, during El Niño events both the SEC and cold tongue weaken dramatically, and TIWs are found to be absent (Baturin and Niiler, 1997). It is possible that the TISO-generated Kelvin waves have an effect on TIWs, by increasing eastward current speeds on the equator. Giese and Harrison (1991) found that in their OGCM the resulting increase in meridional shear amplified the TIWs and produced a transient equatorward heat flux that was as large as the zonal advective warming due to the Kelvin wave.

Equatorward heat flux due to TIW mixing across the sharp SST front is a first-order term in the low-frequency east Pacific heat balance, as large as upwelling or surface fluxes (Hansen and Paul, 1984; Bryden and Brady, 1989; Kessler *et al.*, 1998; Swenson and Hansen, 1999; Wang and McPhaden, 1999). In the annual cycle it tends to counter the cooling due to wind-driven upwelling, which is also largest in June–December. The TIWs accomplish a substantial momentum flux as well, by mixing the shear between the SEC and EUC. The magnitude of mean zonal transport due to this poleward flux of eastward momentum is comparable to the wind-driven Sverdrup transport (Kessler *et al.*, 2003). Thus, the TIWs pose a substantial sampling challenge for observations, and a corresponding requirement for high temporal resolution in the diagnosis of ocean models, in order to properly represent these very large rectified signatures.

With the advent of high-resolution scatterometer winds, the cusp-like TIW SST pattern was found to be imprinted on the cross-equatorial south-easterlies of the

eastern equatorial Pacific (Chelton *et al.*, 2001). This occurs because cold tongue SST stabilizes and decouples the atmospheric planetary boundary layer from the free atmosphere above, leading to a slow surface wind speed. As the south-easterlies blow across the distorted front and over warm SST, convection develops that mixes momentum downward and increases the windspeed. Chelton *et al.* (2001) showed that because the wind direction is quite consistent, this feedback produces a systematically positive curl and divergence signal along the SST front, raising the possibility of a coupled interaction that could further impact the ocean.

6.7.3 ISV outside the equatorial Indo-Pacific

Large intraseasonal signatures are prominent in several regions outside the equatorial Indo-Pacific that are unconnected to the TISO signals that form the main subject of this book. This large topic is sketched here very briefly, giving the bare picture with recent references for those who wish to delve more deeply.

ISV associated with western boundary currents

The poleward western boundary currents closing the Atlantic, Pacific, and South Indian Ocean subtropical gyres generate significant variability in the intraseasonal to interannual frequency bands (Figure 6.12). (The North Indian Ocean is discussed below.) ISV associated with western boundary currents has its origin in the fact that when these currents separate from the coast and are injected into the relatively quiescent open ocean, the strong jets become unstable and form meanders which may grow to become closed-core eddies or rings containing water pinched off from north or south of the jet axis. Bottom topography is an important influence on the path of the current and the regions of meander formation. Rings have scales of a few hundred kilometers, reach depths of more than one kilometer, and may persist for several years as identifiable water mass features. Each of these currents sheds typically three to ten rings each year, resulting in an apparent intraseasonal timescale. Once generated, the rings tend to drift westward with some characteristics of Rossby wave dynamics, though non-linear terms are usually significant, and they can also be swept eastward with the current or reabsorbed by it. Because the rings "contain" the water within them, substantial transport of heat and water properties can be accomplished by this drift. Such western boundary current ISV is seen in Figure 6.12 at the separation regions of the Gulf Stream and Brazil Current in the Atlantic, the Kuroshio and East Australia Current in the Pacific, and the Mozambique/Agulhas Current in the South Indian Ocean. Useful overviews of western boundary current structure and eddy generation mechanisms can be found in Olson (1991), Hogg and Johns (1995), and Ridgway and Dunn (2003). Recent analyses of eddies in the various regions include Qiu (2002), Ducet and LeTraon (2001), Tilburg *et al.* (2001), Goni and Wainer (2001), and Willson and Rees (2000).

The Mozambique/Agulhas Current system differs from the others because the South Indian Ocean subtropical gyre extends south of the Cape of Good Hope, and as a result the western boundary current cannot close the gyre within the Indian

basin. According to linear Sverdrup theory, the western boundary current would extend across the South Atlantic to the coast of South America (Godfrey, 1989), but this is not realized because of the instability of the strong jet injected into the South Atlantic, combined with the background eastward flow around the Southern Ocean. The Agulhas Current retroflects, or turns around, developing an eddy at its western loop; this pinches off and the eddy usually drifts north-westward into the South Atlantic, accomplishing a large water property transport into that ocean, and producing the ISV maximum south of Africa in Figure 6.12. Agulhas eddies are discussed by Schouten *et al.* (2002) and references cited therein.

The Somali Current is distinguished from the other poleward western boundary currents by being present for only part of the year (see the May and August panels of Figure 6.10), a consequence of the fact that winds over the North Indian Ocean do not consist of permanent tropical trades and mid-latitude westerlies, and thus this basin does not have a permanent subtropical gyre. Nevertheless, during the intense summer monsoon winds, the western boundary current that arises along the Somali coast is comparable in speed and transport to the other major systems. ISV associated with the Somali Current is again due to instabilities as it turns offshore near 5°N, as well as further eddies near the tip of Somalia known as the Great Whirl and Socotra Eddy that are spun up with the boundary current (Figure 6.12). Schott and McCreary (2001) provide a comprehensive review of the Somali Current and its stationary and transient eddies.

ISV in the Southern Ocean

A strip of high ISV runs along the axis of the Antarctic Circumpolar Current (ACC; Figure 6.12), where meridional eddy fluxes have long been seen as a principal process of both its heat and momentum balance (Bryden, 1983). Eddy kinetic energy along this band is the most energetic in the world ocean. The poleward heat transport across the Southern Ocean required to maintain steady state is large, and because there are no meridional boundaries to support a gyre circulation, the eddies are the dominant mechanism by which this is accomplished (Gille, 2003). Zonal momentum from the strong and persistent westerly winds must be removed, presumably by vertical transport to be balanced by topographic drag, however, there has been considerable debate about whether eddy momentum fluxes accelerate or decelerate the mean flow (e.g., Morrow *et al.*, 1994; Hughes and Ash, 2001). The ACC appears to be broken up into interleaved jets that flow along quasi-permanent temperature and salinity fronts, some of which are evident at the surface (Belkin and Gordon, 1996). This complex structure tends to be anchored to topography, and much of the eddy variance is generated as the strong, nearly barotropic current flows over bottom features (Morrow *et al.*, 1992). Regions of intense eddy generation are visible in Figure 6.12, and include the ridges south of New Zealand, Drake Passage, and the mid-ocean ridges in the central Indian and Pacific Oceans.

Because of the extreme difficulty of working in these distant and dangerous waters, much of the early work on Southern Ocean eddies took place in Drake Passage where a decades-long observational program took place (Bryden, 1983),

but since satellite altimetry has allowed the production of maps of SSH variability, statistics of the global picture have become possible (Morrow *et al.*, 1992, 1994; Gille and Kelly, 1996). Although the large-scale wind forcing might be expected to produce a large-scale response, Southern Ocean SSH variance is dominated by scales less than 1,000 km. Timescales were found to be about 34 days (Gille and Kelly, 1996). It is not known what produces this frequency structure.

ISV due to baroclinic instability

Currents on the westward limb (equatorial side) of the subtropical gyres (i.e., the North and South Equatorial Currents) in all the oceans typically present conditions favorable to the development of baroclinic instability. At the surface, especially in winter, temperatures are cooler with increasing latitude, but at thermocline level temperatures become warmer moving poleward into the deep bowls of the gyres. The resulting poleward tilt of the gyres with depth implies a change of sign in the vertical of the meridional gradient of potential vorticity, which is a necessary (though not sufficient) condition for such instabilities to grow (see Pedlosky, 1987, for a review of these dynamics). Linear stability analysis suggests that such disturbances should have the preferred size of 2π times the first baroclinic mode Rossby radius (a few hundred kilometers in the subtropics) and disperse as baroclinic Rossby waves; these characteristics will produce an intraseasonal timescale in subtropical time series (Qiu, 1999). Two such regions stand out in the high-passed SSH variability map of Figure 6.12: in the eastern Indian Ocean along 12°S, and in the western Pacific Ocean along 20°N. In both cases, although these are regions potentially influenced by intraseasonal wind and heat flux forcing, the prominent ISV maxima have been shown to be due to internal oceanic phenomena, unconnected to TISO.

The band of high ISV roughly along 12°S in the Indian Ocean (Figure 6.12) occurs along the axis of the westward SEC, which carries low-salinity Pacific water from the ITF into the central Indian Ocean. Feng and Wijffels (2002) showed that the high-variance signal shown in Figure 6.12 has a strong seasonal modulation, being larger by a factor of about two in July–September when the SEC itself is largest (as is the ITF which partly feeds it). They noted that this seasonality is inconsistent with the ISV forced by equatorial winds, which brings strong ISV to the Indonesian coast via Kelvin wave propagation, but peaks in January–June (see Section 6.6). Instead, the ISV observed along 12°S was found to be an internally-generated baroclinic instability of the SEC itself. Feng and Wijffels (2002) showed propagating sea level features, arising near 115°E, with a period of 40–80 days, a length-scale of 100–150 km, and a westward phase speed of 15–19 cm s^{-1}, consistent with the first-mode baroclinic Rossby wave speed in this region, and concluded that the observed ISV maximum was produced as an internal instability in the ocean.

A band of high ISV extends along 20°N from Hawaii to Taiwan (Figure 6.12), following the path of the eastward Subtropical Countercurrent (STCC) in the North Pacific. The STCC overlies the subsurface part of the westward North Equatorial Current (NEC) which extends poleward to the center of the gyre at thermocline level. As in the Indian Ocean signal discussed above, the 20°N ISV has a pronounced

seasonal modulation, with its maximum in boreal spring about 50% larger than its boreal fall minimum (Qiu, 1999). Qiu showed that as the vertical shear between the STCC and the NEC increases in boreal winter, the vertical-meridional structure becomes baroclinically unstable and eddies develop. Roemmich and Gilson (2001) used temperature profiles along a ship track roughly at 20°N to show that their subsurface structure produced an overturning circulation and substantial poleward heat flux. The eddies propagate westward as baroclinic Rossby waves with a phase speed of about $10\,\mathrm{cm\,s^{-1}}$ and wavelength of about 500 km, thus a period of about 60 days. Although there is substantial intraseasonal forcing in this region, it occurs primarily in boreal summer, and the ISV maximum seen in Figure 6.12 appears to be due to internal ocean processes.

6.8 CONCLUSION

The literature reviewed here has shown that tropical intraseasonal forcing leads to a wide complex of dynamic and thermodynamic effects in the ocean, some of which have the potential to produce subsequent effects on the evolution of the tropical climate system. A principal driver of present enthusiasm for tropical oceanic ISV has been the possibility of oceanic rectification leading to a connection between the MJO and the ENSO cycle, but the recent progress in observing and modeling the eastern Indian Ocean and the development of the Asian monsoon suggests that some of the same mechanisms might be operating there as well.

The MJO/ENSO question revolves around the still-unquantified net effect of intraseasonally-oscillating forcing on the west Pacific warm pool. As reviewed in Sections 6.2 and 6.3, it is clear that the results of TISO heat, moisture, and wind forcing, profoundly affect the character and composition of the west Pacific warm pool, producing its commonly stacked velocity structure with several layers of reversing jets and its frequent salinity-stratified barrier layer. These dynamic and thermodynamic consequences are tied together because the result of precipitation is to enhance the response to wind forcing by concentrating it in a thin surface layer. While the possibilities for rectification are rife, the quantification of suggested mechanisms is hindered by the difficulty of modeling these processes, which depend sensitively on the mixed layer depth and the vertical structure of momentum mixing, among the least believable aspects of present-generation OGCMs. Indeed, similar models come to opposite conclusions about even the sign of some of the important rectified terms (e.g., the sign of the rectified current in the model of Kessler and Kleeman, 2000, compared to that of Waliser *et al.*, 2003). In addition, the paucity of salinity observations means that the spatial structure of the mixed and barrier layers is barely known.

A quantitative description of Indian Ocean ISV is only recently being realized through programs such as JASMINE (Webster *et al.*, 2002) and the maintenance of moored time series in the Bay of Bengal. Since the role of salinity stratification is likely to be even more intense than in the Pacific, we can expect that complex vertical structures, with the consequent creation of oceanic memory of intraseasonal forcing

and resulting potential for feedback and rectification will turn out to be important in the evolution of Indian Ocean climate as well.

6.9 REFERENCES

Anderson, S. P., R. A. Weller, and R. B. Lukas (1996) Surface buoyancy forcing and the mixed layer of the western equatorial Pacific warm pool: Observations and 1S model results. *J. Climate*, **9**, 3056–3085.

Annamalai, H., R. Murtugudde, J. Potemra, S. P. Xie, P. Liu, and B. Wang (2003) Coupled dynamics over the Indian Ocean: Spring initiation of the Zonal Mode. *Deep-Sea Res. II*, **50**, 2305–2330.

Barnston, A. G., Y. He, and D. A. Unger (2000) A forecast product that maximizes utility for state-of-the-art seasonal climate prediction. *Bull. Amer. Meteorol. Soc.*, **81**, 1271–1290.

Baturin, N. G. and P. P. Niiler (1997) Effects of instability waves in the mixed layer of the equatorial Pacific. *J. Geophys. Res.*, **102**, 21771–21793.

Belamari, S., J.-L. Redelsperger, and M. Pontaud (2003) Dynamic role of a westerly wind burst in triggering an equatorial Pacific warm event. *J. Climate*, **16**, 1869–1890.

Belkin, I. M. and A. L. Gordon (1996) Southern Ocean fronts from the Greenwich Meridian to Tasmania. *J. Geophys. Res. Oceans*, **101**, 3675–3696.

Bhat, G. S., S. Gadgil, P. V. H. Kumar, S. R. Kalsi, P. Madhusoodanan, V. S. N. Murty, C. V. K. P. Rao, V. R. Babu, L. V. G. Rao, and R. R. Raos (2001) BOBMEX: The Bay of Bengal monsoon experiment. *Bull. Amer. Meteorol. Soc.,* **82**, 2217–2243.

Blanke, B. and S. Raynaud (1997) Kinematics of the Pacific equatorial undercurrent: An Eulerian and Lagrangian approach from GCM results. *J. Phys. Oceanogr.*, **27**, 1038–1053.

Bryden, H. L. (1983) The Southern Ocean. In: A. R. Robinson (ed.), *Eddies in Marine Science*, Springer-Verlag, New York, pp. 265–277.

Bryden, H. L. and E. C. Brady (1989) Eddy momentum and heat fluxes and their effects on the circulation of the equatorial Pacific Ocean. *J. Mar. Res.*, **47**, 55–79.

Busalacchi, A. J. and M. A. Cane (1985) Hindcasts of sea level variations during the 1982–83 El Niño. *J. Phys. Oceanogr.*, **15**, 213–221.

Chelton, D. B., S. K. Esbensen, M. G. Schlax, N. Thum, M. H. Freilich, F. J. Wentz, C. L. Gentemann, M. J. McPhaden, and P. S. Schopf (2001) Observations of coupling between surface wind stress and sea surface temperature in the eastern tropical Pacific. *J. Climate*, **14**, 1479–1498.

Chelton, D. B., M. H. Freilich, and S. K. Esbensen (2000a) Satellite observations of the wind jets off the Pacific coast of Central America. Part I: Case studies and statistical characteristics. *Mon. Wea. Rev.*, **128**, 1993–2018.

Chelton, D. B., M. H. Freilich, and S. K. Esbensen (2000b) Satellite observations of the wind jets off the Pacific coast of Central America. Part II: Regional relationships and dynamical considerations. *Mon. Wea. Rev.*, **128**, 2019–2043.

Chelton, D. B., F. J. Wentz, C. L. Gentemann, R. A. deSzoeke, and M. G. Schlax (2000c) Satellite microwave SST observation of transequatorial Tropical Instability Waves. *Geophys. Res. Lett.*, **27**, 1239–1242.

Chelton, D. B., M. G. Schlax, J. M. Lyman, and G. C. Johnson (2003) Equatorially trapped Rossby waves in the presence of meridionally sheared baroclinic flow in the Pacific Ocean. *Prog. Oceanogr.*, **56**, 323–380.

Clarke, A. J. (1994) Why are surface equatorial ENSO winds anomalously westerly under anomalous large-scale convection? *J. Climate*, **7**, 1623–1627.

Clarke, A. J. and R. Ahmed (1999) Dynamics of remotely forced intraseasonal oscillations off the western coast of South America. *J. Phys. Oceanogr.*, **29**, 240–258.

Contreras, R. F. (2002) Long-term observations of tropical instability waves. *J. Phys. Oceanogr.*, **32**, 2715–2722.

Cox, M. D. (1980) Generation and propagation of 30-day waves in a numerical model of the Pacific. *J. Phys. Oceanogr.*, **10**, 1168–1186.

Cravatte, S., J. Picaut, and G. Eldin (2003) Second and first baroclinic modes in the equatorial Pacific at intraseasonal timescales. *J. Geophys. Res.*, **108**, 3226, doi:10.1029/2002JC001511.

Cronin, M. F. and M. J. McPhaden (1997) The upper ocean heat balance in the western equatorial Pacific warm pool during September–December 1992. *J. Geophys. Res.*, **102**, 8533–8553.

Cronin, M. F. and M. J. McPhaden (2002) Barrier layer formation during westerly wind bursts. *J. Geophys. Res.*, **107**, 8020, doi:10.1029/2001JC001171.

Cronin, M. F., M. J. McPhaden, and R. H. Weisberg (2000) Wind-forced reversing jets in the western equatorial Pacific. *J. Phys. Oceanogr.*, **30**, 657–676.

Delcroix, T., G. Eldin, M. J. McPhaden, and A. Morliere (1993) Effects of westerly wind bursts upon the western equatorial Pacific Ocean, February–April 1991. *J. Geophys. Res.*, **98**, 16379–16385.

Ducet, N. and P. Y. LeTraon (2001) A comparison of surface eddy kinetic energy and Reynolds stresses in the Gulf Stream and the Kuroshio Current systems from merged TOPEX/Poseidon and ERS-1/2 altimetric data. *J. Geophys. Res.*, **106**, 16603–16662.

Durland, T. S. and B. Qiu (2003) Transmission of subinertial Kelvin waves through a strait. *J. Phys. Oceanogr.*, **33**, 1337–1350.

Eigenheer, A. and D. Quadfasel (2000) Seasonal variability of the Bay of Bengal circulation inferred from TOPEX/Poseidon altimetry. *J. Geophys. Res.*, **105**, 3243–3252.

Eldin, G., T. Delcroix, C. Henin, K. Richards, Y. duPenhoat, J. Picaut, and P. Rual (1994) Large-scale current and thermohaline structures along 156° during the COARE intensive observing period. *Geophys. Res. Lett.*, **21**, 2681–2684.

Enfield, D. B. (1987) The intraseasonal oscillation in eastern Pacific sea levels: How is it forced? *J. Phys. Oceanogr.*, **17**, 1860–1876.

Enfield, D. B. and R. Lukas (1983) Low-frequency sea level variability along the South American coast in 1981–83. *Trop. Ocean-Atmos. Newslett.*, **28**, 2–4.

Fedorov, A. V. (2002) The response of the coupled tropical ocean–atmosphere to westerly wind bursts. *Quart. J. Royal Meteorol. Soc.*, **128**, 1–23.

Feng, M. and S. Wijffels (2002) Intraseasonal variability in the South Equatorial Current of the east Indian Ocean. *J. Phys. Oceanogr.*, **32**, 265–277.

Fink, A. and P. Speth (1997) Some potential forcing mechanisms of the year-to-year variability of the tropical convection and its intraseasonal (25–70-day) variability. *Int. J. Climatol.*, **17**, 1513–1534.

Flament, P. J., S. C. Kennan, R. A. Knox, P. P. Niiler, and R. L. Bernstein (1996) The three-dimensional structure of an upper-ocean vortex in the tropical Pacific Ocean. *Nature*, **383**, 610–613.

Fu, L.-L., E. J. Christensen, C. A. Yamarone, M. Lefebvre, Y. Menard, M. Dorrer, and P. Escudier (1994) TOPEX/POSEIDON mission overview. *J. Geophys. Res.*, **99**, 24369–24382.

Giese, B. S. and D. E. Harrison (1990) Aspects of the Kelvin wave response to episodic wind forcing. *J. Geophys. Res. Oceans*, **95**, 7289–7312.

Giese, B. S. and D. E. Harrison (1991) Eastern equatorial Pacific response to three composite westerly wind types. *J. Geophys. Res.*, **96**, 3239–3248.

Giese, B. S., J. A. Carton, and L. J. Holl (1994) Sea level variability in the eastern Pacific as observed by TOPEX and Tropical Ocean Global–Atmosphere Tropical Atmosphere–Ocean experiment. *J. Geophys. Res.*, **99**, 24739–24748.

Gille, S. T. (2003) Float observation of the Southern Ocean. Part II: Eddy fluxes. *J. Phys. Oceanogr.*, **33**, 1182–1196.

Gille, S. T. and K. A. Kelly (1996) Scales of spatial and temporal variability in the Southern Ocean. *J. Geophys. Res.*, **101**, 8759–8773.

Godfrey, J. S. (1989) A Sverdrup model of the depth-integrated flow for the world ocean, allowing for island circulations. *Geophys. Astrophys. Fluid Dyn.*, **45**, 89–112.

Godfrey, J. S., R. A. Houze, R. H. Johnson, R. Lukas, J.-L. Redelsperger, A. Sumi, and R. Weller (1998) Coupled Ocean-Atmosphere Response Experiment (COARE): An interim report. *J. Geophys. Res.*, **103**, 14395–14450.

Goni, G. J. and I. Wainer (2001) Investigation of the Brazil Current front variability from altimeter data. *J. Geophys. Res.*, **106**, 31117–31128.

Gould, J., D. Roemmich, S. Wijffels, H. Freeland, M. Ignaszewsky, X. Jianping, S. Pouliquen, Y. Desaubies, U. Send, and K. Radhakrishman (2004) Argo profiling floats bring new era of in situ ocean observations. *EOS*, **85**, 179–191.

Gutzler, D. S. (1991) Interannual fluctuations of intraseasonal variance of near-equatorial zonal winds. *J. Geophys. Res.*, **96**, 3173–3185.

Halpern, D., R. A. Knox, and D. S. Luther (1988) Observations of 20-day period meridional current oscillations in the upper ocean along the Pacific equator. *J. Phys. Oceanogr.*, **18**, 1514–1534.

Han, W., J. P. McCreary, D. L. T. Anderson, and A. J. Mariano (1999) On the dynamics of the eastward surface jets in the equatorial Indian Ocean. *J. Phys. Oceanogr.*, **29**, 2191–2209.

Han, W., D. M. Lawrence, and P. J. Webster (2001a) Dynamical response of equatorial Indian Ocean to intraseasonal winds: Zonal flow. *Geophys. Res. Lett.*, **28**, 4215–4218.

Han, W., J. P. McCreary, and K. E. Kohler (2001b) Influence of precipitation minus evaporation and Bay of Bengal rivers on dynamics, thermodynamics, and mixed layer physics in the upper Indian Ocean. *J. Geophys. Res.*, **106**, 6895–6916.

Hansen, D. V. and G. A. Maul (1991) Anticyclonic current rings in the eastern tropical Pacific Ocean. *J. Geophys. Res.*, **96**, 6965–6979.

Hansen, D. V. and C. A. Paul (1984) Genesis and effect of long waves in the equatorial Pacific. *J. Geophys. Res.*, **89**, 10431–10440.

Hayes, S. P., L. J. Mangum, J. Picaut, A. Sumi, and K. Takeuchi (1991) TOGA-TAO: A moored array for real-time measurements in the tropical Pacific Ocean. *Bull. Amer. Meteorol. Soc.*, **72**, 339–347.

Hendon, H. H. and M. L. Salby (1994) The life cycle of the Madden–Julian Oscillation. *J. Atmos. Sci.*, **51**, 2225–2231.

Hendon, H. H., B. Liebmann, and J. D. Glick (1998) Oceanic Kelvin waves and the Madden–Julian Oscillation. *J. Atmos. Sci.*, **55**, 88–101.

Hendon, H. H., C. Zhang, and J. D. Glick (1999) Interannual variability of the Madden–Julian Oscillation during austral summer. *J. Climate*, **12**, 2358–2550.

Hisard, P., J. Merle, and B. Voituriez (1970) The equatorial undercurrent observed at 170°E in March and April 1967. *J. Mar. Res.*, **28**, 281–303.

Hogg, N. G. and W. E. Johns (1995) Western boundary currents. *Rev. Geophys.*, **33**, 1311–1334.

Hormazabal, S., G. Shaffer, J. Letelier, and O. Ulloa (2001) Local and remote forcing of sea surface temperature in the coastal upwelling system off Chile. *J. Geophys. Res. Oceans*, **106**(C8), 16657–16671.

Hormazabal, S., G. Shaffer, and O. Pizarro (2002) Tropical Pacific control of intraseasonal oscillations off Chile by way of oceanic and atmospheric pathways. *Geophys. Res. Lett.*, **29**, Art 1081.

Hughes, C. W. and E. R. Ash (2001) Eddy forcing of the mean flow in the Southern Ocean. *J. Geophys. Res.*, **106**, 2713–2722.

Hurd, W. E. (1929) Northers of the Gulf of Tehuantepec. *Mon. Wea. Rev.*, **57**, 192–194.

Jensen, T. G. (1993) Equatorial variability and resonance in a wind-driven Indian Ocean model. *J. Geophys. Res.*, **98**, 22533–22552.

Johnson, E. S. and D. S. Luther (1994) Mean zonal momentum balance in the upper and central equatorial Pacific Ocean. *J. Geophys. Res.*, **99**, 7689–7705.

Johnson, E. S. and M. J. McPhaden (1993a) Structure of intraseasonal Kelvin waves in the equatorial Pacific Ocean. *J. Phys. Oceanogr.*, **23**, 608–625.

Johnson, E. S. and M. J. McPhaden (1993b) Effects of a 3-dimensional mean flow on intraseasonal Kelvin waves in the equatorial Pacific Ocean. *J. Geophys. Res. Oceans*, **98**, 10185–10194.

Johnson, G. C., M. J. McPhaden, and E. Firing (2001) Equatorial Pacific Ocean horizontal velocity, divergence and upwelling. *J. Phys. Oceanogr.*, **31**, 839–849.

Johnson, G. C., B. M. Sloyan, W. S. Kessler, and K. E. McTaggart (2002) Direct measurements of upper ocean currents and water properties across the equatorial Pacific during the 1990s. *Prog. Oceanogr.*, **52**, 31–61.

Kessler, W. S. (2001) EOF representations of the Madden–Julian Oscillation and its connection with ENSO. *J. Climate*, **14**, 3055–3061.

Kessler, W. S. (2002a) Mean three-dimensional circulation in the northeast tropical Pacific. *J. Phys. Oceanogr.*, **32**, 2457–2471.

Kessler, W. S. (2002b) Is ENSO a cycle or a series of events? *Geophys. Res. Lett.*, **29**, 2125, doi:1029/2002GL015924.

Kessler, W. S. and R. Kleeman (2000) Rectification of the Madden–Julian Oscillation into the ENSO cycle. *J. Climate*, **13**, 3560–3575.

Kessler, W. S. and M. J. McPhaden (1995a) Oceanic equatorial waves and the 1991–93 El Niño. *J. Climate*, **8**, 1757–1774.

Kessler, W. S. and M. J. McPhaden (1995b) The 1991–93 El Niño in the central Pacific. *Deep-Sea Res., II*, **42**, 295–333.

Kessler, W. S., G. C. Johnson, and D. W. Moore (2003) Sverdrup and nonlinear dynamics of the Pacific equatorial currents. *J. Phys. Oceanogr.*, **33**, 994–1008.

Kessler, W. S., M. J. McPhaden, and K. M. Weickmann (1995) Forcing of intraseasonal Kelvin waves in the equatorial Pacific. *J. Geophys. Res.*, **100**, 10613–10631.

Kessler, W. S., L. M. Rothstein, and D. Chen (1998) The annual cycle of SST in the eastern tropical Pacific, diagnosed in an ocean GCM. *J. Climate*, **11**, 777–799.

Kindle, J. C. and P. A. Phoebus (1995) The ocean response to operational wind bursts during the 1991–92 El Niño. *J. Geophys. Res.*, **100**, 4803–4920.

Kindle, J. C. and J. D. Thompson (1989) The 26- and 50-day oscillations in the western Indian Ocean: Model results. *J. Geophys. Res.*, **94**, 4721–4736.

Kutsuwasa, K. and M. J. McPhaden (2002) Intraseasonal variations in the upper equatorial Pacific Ocean prior to and during the 1997–98 El Niño. *J. Phys. Oceanogr.*, **32**(4), 1133–1149.

Lagerloef, G. S. E., G. T. Mitchum, R. B. Lukas, and P. P. Niiler (1999) Tropical Pacific near-surface currents estimated from altimeter, wind and drifter data. *J. Geophys. Res.*, **104**, 23313–23326.

Latif, M., J. Biercamp, and H. von Storch (1988) The response of a coupled ocean–atmosphere general circulation model to wind bursts. *J. Atmos. Sci.*, **45**, 964–979.

Legeckis, R. (1977) Long waves in the eastern equatorial ocean: A view from a geostationary satellite. *Science*, **197**, 1179–1181.

Lengaigne, M., J. P. Boulanger, C. Menkes, S. Masson, G. Madec, and P. Delecluse (2002) Ocean response to the March 1997 westerly wind event. *J. Geophys. Res. (O)*, **107**(C12): art. no. 8015.

Levitus, S. (1994) Climatological Atlas of the World Ocean, NOAA Prof. Pap. No. 13. US Government Printing Office.

Loschnigg, J. and P. J. Webster (2000) A coupled ocean-atmosphere system of SST modulation for the Indian Ocean. *J. Climate*, **13**, 3342–3360.

Lukas, R. and E. Lindstrom (1991) The mixed layer of the western equatorial Pacific. *J. Geophys. Res.*, **96**, 3343–3357.

Lukas, R., S. P. Hayes, and K. Wyrtki (1984) Equatorial sea level response during the 1982–1983 El Niño. *J. Geophys. Res.*, **89**, 10425–10430.

Luther, D. S. and E. S. Johnson (1990) Eddy energetics in the upper equatorial Pacific during the Hawaii-to-Tahiti Shuttle Experiment. *J. Phys. Oceanogr.*, **20**, 913–944.

Luyten, J. R. and D. H. Roemmich (1982) Equatorial currents at semi-annual period in the Indian Ocean. *J. Phys. Oceanogr.*, **12**, 406–413.

Madden, R. A. and P. A. Julian (1994) Observations of the 40–50-day tropical oscillation – A review. *Mon. Wea. Rev.*, **122**, 814–837.

Mariano, A. J., E. H. Ryan, B. D. Perkins, and S. Smithers (1995) The mariano global surface velocity analysis 1.0. U.S. Coast Guard Technical Report, CG-D-34-95.

Masina, S. and S. G. H. Philander (1999) An analysis of tropical instability waves in a numerical model of the Pacific Ocean. Part 1: Spatial variability of the waves. *J. Geophys. Res.*, **104**, 29613–29635.

Masina, S., S. G. H. Philander, and A. B. G. Bush (1999) An analysis of tropical instability waves in a numerical model of the Pacific. Ocean. Part 2: Generation and energetics of the waves. *J. Geophys. Res.*, **104**, 29637–29661.

Masson, S., P. Delecluse, J.-P. Boulanger, and C. Menkes (2002) A model study of the seasonal variability and formation mechanisms of the barrier layer in the eastern equatorial Indian Ocean. *J. Geophys. Res.*, **107**, 8017, doi:10.1029/2001JC000832.

Masson, S., P. Delecluse, and J.-P. Boulanger (2003) Impacts of salinity on the eastern Indian Ocean during the termination of the fall Wyrtki Jet. *J. Geophys. Res.*, **108**, doi:10.1029/2001JC00083.

McClain, C. R., J. R. Christian, S. R. Signorinin, M. R. Lewis, I. Asanuma, D. Turk, and C. Dupouy-Douchement (2002) Satellite ocean color observations of the tropical Pacific Ocean. *Deep-Sea Res. II*, **49**, 2533–2560.

McCreary, J. P. (1984) Equatorial beams. *J. Mar. Res.*, **42**, 395–430.

McCreary, J. P. (1985) Modeling equatorial ocean circulation. *Ann. Rev. Fluid Mech.*, **17**, 359–409.

McCreary, J. P., P. K. Kundu, and R. L. Molinari (1993) A numerical investigation of dynamics, thermodynamics and mixed-layer processes in the Indian Ocean. *Prog. Oceanogr.*, **31**, 181–244.

McCreary, J. P., H. S. Lee, and D. B. Enfield (1989) Response of the coastal ocean to strong offshore winds: With application to circulations in the Gulf of Tehuantepec and Papagayo. *J. Mar. Res.*, **47**, 81–109.

McPhaden, M. J. (1995) The Tropical Atmosphere–Ocean array is completed. *Bull. Amer. Meteorol. Soc.*, **76**, 739–741.

McPhaden, M. J. (1996) Monthly period oscillations in the Pacific North Equatorial Countercurrent. *J. Geophys. Res.*, **101**, 6337–6360.

McPhaden, M. J. (1999) Genesis and evolution of the 1997–98 El Niño. *Science*, **283**, 950–954.

McPhaden, M. J. (2002) Mixed layer temperature balance on intraseasonal timescales in the equatorial Pacific Ocean. *J. Climate*, **15**, 2632–2647.

McPhaden, M. J. and S. P. Hayes (1991) On the variability of winds, sea surface temperature and surface layer heat content in the western equatorial Pacific. *J. Geophys. Res.*, **96**(suppl.), 3331–3342.

McPhaden, M. J. and B. A. Taft (1988) Dynamics of seasonal and intraseasonal variability in the eastern equatorial Pacific. *J. Phys. Oceanogr.*, **18**, 1713–1732.

McPhaden, M. J., H. P. Freitag, S. P. Hayes, B. A. Taft, Z. Chen, and K. Wyrtki (1988) The response of the equatorial Pacific Ocean to a westerly wind burst in May 1986. *J. Geophys. Res.*, **93**, 10589–10603.

McPhaden, M. J., S. P. Hayes, L. J. Mangum, and J. M. Toole (1990) Variability in the western equatorial Pacific Ocean during the 1986–87 El Niño/Southern Oscillation event. *J. Phys. Oceanogr.*, **20**, 190–208.

McPhaden, M. J., F. Bahr, Y. duPenhoat, E. Firing, S. P. Hayes, P. P. Niiler, P. L. Richardson, and J. M. Toole (1992) The response of the western equatorial Pacific Ocean to westerly wind bursts during Novermber 1989 to January 1990. *J. Geophys. Res.*, **97**, 14289–14303.

McPhaden, M. J. and X. Yu (1999) Equatorial waves and the 1997–98 El Niño. *Geophys. Res. Lett.*, **26**, 2961–2964.

Metzger, E. J., H. E. Hurlburt, J. C. Kindle, Z. Sirkes, and J. M. Pringle (1992) Hindcasting of wind-driven anomalies using a reduced gravity global ocean model. *Mar. Tech. Soc. J.*, **26**, 23–32.

Meyers, G., J.-R. Donguy, and R. Reed (1986) Evaporative cooling of the western equatorial Pacific. *Nature*, **312**, 258–260.

Miyama, T., J. P. McCreary, T. G. Jensen, J. Loschnigg, S. Godfrey, and A. Ishida (2003) Structure and dynamics of the Indian Ocean cross-equatorial cell. *Deep-Sea Res., II*, **50**, 2023–2047.

Moore, A. M. and R. Kleeman (1999) Stochastic forcing of ENSO by the intraseasonal oscillation. *J. Climate*, **12**, 1199–1220.

Moore, A. M. and R. Kleeman (2001) The differences between the optimal perturbations of coupled models of ENSO. *J. Climate*, **14**, 138–163.

Moore, D. W. and J. P. McCreary (1990) Excitation of intermediate-frequency equatorial waves at a western ocean boundary: With application to observations from the Indian Ocean. *J. Geophys. Res.*, **95**, 5219–5231.

Morrow, R., J. Church, R. Coleman, D. Chelton, and N. White (1992) Eddy momentum flux and its contribution to the Southern Ocean momentum balance. *Nature*, **357**, 482–484.

Morrow, R., R. Coleman, J. Church, and D. Chelton (1994) Surface eddy momentum flux and velocity variances in the Southern Ocean from Geosat altimetry. *J. Phys. Oceanogr.*, **24**, 2050–2071.

Müller-Karger, F. E. and C. Fuentes-Yaco (2000) Characteristics of wind-generated rings in the eastern tropical Pacific Ocean. *J. Geophys. Res.*, **105**, 1271–1284.

Murtugudde, R. and A. J. Busalacchi (1999) Interannual variability of the dynamics and thermodynamics of the tropical Indian Ocean. *J. Climate*, **12**, 2300–2326.

Murtugudde, R., J. P. McCreary, and A. J. Busalacchi (2000) Oceanic processes associated with anomalous events in the Indian Ocean with relevance to 1997–1998. *J. Geophys. Res.*, **105**, 3295–3306.

Musman, S. (1989) Sea height wave form in equatorial waves and its interpretation. *J. Geophys. Res.*, **94**, 3303–3309.

Neelin, J. D., D. S. Battisti, A. C. Hirst, F.-F. Jin, Y. Wakata, T. Yamagata, and S. E. Zebiak (1998) ENSO theory. *J. Geophys. Res.*, **103**, 14261–14290.

Olson, D. B. (1991) Rings in the ocean. *Ann. Rev. Earth Planet Sci.*, **19**, 283–311.

Pedlosky, J. (1987) *Geophysical Fluid Dynamics* (2nd edition). Springer-Verlag, New York. 710 pp.

Perigaud, C. (1990) Sea level oscillations observed with Geosat along the two shear fronts of the Pacific North Equatorial Countercurrent. *J. Geophys. Res.*, **95**, 7239–7248.

Philander, S. G. H. (1976) Instabilities of zonal equatorial currents. *J. Geophys. Res.*, **81**, 3725–3735.

Philander, S. G. H. (1978) Instabilities of zonal equatorial currents, 2. *J. Geophys. Res.*, **83**, 3679–3682.

Philander, S. G. H. and R. C. Pacanowski (1980) The generation of equatorial currents. *J. Geophys. Res.*, **85**, 1123–1136.

Philander, S. G. H., W. J. Hurlin, and R. C. Pacanowski (1986) Properties of long equatorial waves in models of the seasonal cycle in the tropical Atlantic and Pacific Oceans. *J. Geophys. Res.*, **91**, 14207–14211.

Potemra, J. T., S. L. Hautala, J. Sprintall, and W. Pandoe (2002) Interaction between the Indonesian Seas and the Indian Ocean in observations and numerical models. *J. Phys. Oceanogr.*, **32**, 1838–1854.

Potemra, J. T., S. L. Hautala, and J. Sprintall (2003) Vertical structure of the Indonesian Throughflow in a large-scale model. *Deep-Sea Res. II*, **50**, 2143–2161.

Potemra, J. T., M. E. Luther, and J. J. O'Brien (1991) The seasonal circulation of the upper ocean in the Bay of Bengal. *J. Geophys. Res.*, **96**, 12667–12683.

Qiao, L. and R. H. Weisberg (1998) Tropical instability wave energetics: Observations from the Tropical Instability Wave Experiment. *J. Phys. Oceanogr.*, **28**, 345–360.

Qiu, B. (1999) Seasonal eddy field modulation of the North Pacific Subtropical Countercurrent: TOPEX/Poseidon observations and theory. *J. Phys. Oceanogr.*, **29**, 2471–2486.

Qiu, B. (2002) The Kuroshio Extension system: Its large-scale variability and role in the midlatitude ocean–atmosphere interaction. *J. Oceanogr.*, **58**, 57–75.

Qiu, B., M. Mao, and Y. Kashino (1999) Intraseasonal variability in the Indo-Pacific Throughflow and the regions surrounding the Indonesian Seas. *J. Phys. Oceanogr.*, **29**, 1599–1618.

Ralph, E. A., K. Bi, P. P. Niiler, and Y. duPenhoat (1997) A Lagrangian description of the western equatorial Pacific response to the wind burst of December 1992: Heat advection in the warm pool. *J. Climate*, **10**, 1706–1721.

Ramanathan, V. and W. Collins (1991) Thermodynamic regulation of ocean warming by cirrus clouds deduced from observations of the 1987 El Niño. *Nature*, **351**, 27–32.

Raymond, D. J. (2001) A new model of the Madden–Julian Oscillation. *J. Atmos. Sci.*, **58**, 2807–2819.

Reppin, J., F. A. Schott, J. Fischer, and D. Quadfasel (1999) Equatorial currents and transports in the upper central Indian Ocean: Annual cycle and interannual variability. *J. Geophys. Res.*, **104**, 15495–15514.

Reverdin, G. (1987) The upper equatorial Indian Ocean: The climatological seasonal cycle. *J. Phys. Oceanogr.*, **17**, 903–927.

Reverdin, G. and J. Luyten (1986) Near-surface meanders in the equatorial Indian Ocean. *J. Phys. Oceanogr.*, **16**, 1088–1100.

Richardson, R. A., I. G. Ginnis, and L. M. Rothstein (1999) A numerical investigation of the local ocean response to westerly wind burst forcing in the western equatorial Pacific. *J. Phys. Oceanogr.*, **29**, 1334–1352.

Ridgway, K. R. and J. R. Dunn (2003) Mesoscale structure of the mean East Australian Current System and its relationship with topography. *Prog. Oceanogr.*, **56**, 189–222.

Roden, G. I. (1961) On the wind-driven circulation in the Gulf of Tehuantepec and its effect on surface temperatures. *Geofis. Int.*, **1**, 55–72.

Roemmich, D. and J. Gilson (2001) Eddy transport of heat and thermocline waters in the North Pacific: A key to interannual/decadal climate variability? *J. Phys. Oceanogr.*, **31**, 675–687.

Roemmich, D., M. Morris, W. R. Young, and J. R. Donguy (1994) Fresh equatorial jets. *J. Phys. Oceanogr.*, **24**, 540–558.

Roulston, M. S. and J. D. Neelin (2000) The reponse of an ENSO model to climate noise, weather noise and intraseasonal forcing. *Geophys. Res. Lett.*, **27**, 3723–3726.

Saji, N. H., B. N. Goswami, P. N. Vinayachandran, and T. Yamagata (1999) A dipole mode in the tropical Indian Ocean. *Nature*, **401**, 360–363.

Schiller, A. and J. S. Godfrey (2003) Indian Ocean intraseasonal variability in an ocean general circulation model. *J. Climate*, **16**, 21–39.

Schneider, N. (1998) The Indonesian Throughflow and the global climate system. *J. Climate*, **11**, 676–689.

Schott, F. A. and J. P. McCreary (2001) The monsoon circulation of the Indian Ocean. *Prog. Oceanogr.*, **51**, 1–123.

Schott, F., J. Reppin, and J. Fischer (1994) Currents and transports of the Monsoon Current south of Sri Lanka. *J. Geophys. Res.*, **99**, 25127–25141.

Schouten, M. W., W. P. M. de Ruijter, and P. J. van Leeuwen (2002) Upstream control of Agulhas ring shedding. *J. Geophys. Res.*, **107**, doi:10.1029/2001JC000804.

Sengupta, D., R. Senan, and B. N. Goswami (2001) Origin of intraseasonal variability of circulation in the tropical central Indian Ocean. *Geophys. Res. Lett.* **28**, 1267–1270.

Shetye, S. R., A. D. Gouveia, D. Shankar, S. S. C. Shenoi, P. N. Vinayachandran, D. Sundar, G. S. Michael, and G. Nampoothiri (1996) Hydrography and circulation in the western Bay of Bengal during the northeast monsoon. *J. Geophys. Res.*, **101**, 14011–14025.

Shinoda, T. and H. H. Hendon (1998) Mixed layer modeling of intraseasonal variability in the tropical western Pacific and Indian Oceans. *J. Climate*, **11**, 2668–2685.

Shinoda, T. and H. H. Hendon (2001) Upper-ocean heat budget in response to the Madden–Julian oscillation in the western equatorial Pacific. *J. Climate* **14**(21), 4147–4165.

Shinoda, T. and H. H. Hendon (2002) Rectified wind forcing and latent heat flux produced by the Madden–Julian Oscillation. *J. Climate*, **15**(23), 3500–3508.

Shinoda, T., H. H. Hendon, and J. D. Glick (1998) Intraseasonal variability of surface fluxes and sea surface temperature in the tropical western Pacific and Indian Oceans. *J. Climate*, **11**, 1685–1702.

Slingo, J. M., D. P. Rowell, K. R. Sperber, and F. Nortley (1999) On the predictability of the inter annual behavior of the Madden–Julian Oscillation and its relationship with El Niño. *Quart. J. Roy. Met. Soc.*, **125**, 583–609.

Somayajulu, Y. K., V. S. N. Murty, and Y. V. B. Sarma (2003) Seasonal and interannual variability of surface circulation in the bay of Bengal from TOPEX/Poseidon altimetry. *Deep-Sea Res. II*, **50**, 867–880.

Spillane, M. C., D. B. Enfield, and J. S. Allen (1987) Intraseasonal oscillations in sea level along the west coast of the Americas. *J. Phys. Oceanogr.*, **17**, 313–325.

Sprintall, J. and M. J. McPhaden (1994) Surface layer variations observed in multiyear time series measurements from the western equatorial Pacific. *J. Geophys. Res.*, **99**, 963–979.

Sprintall, J., J. T. Potemra, S. L. Hautala, N. A Bray, and W. W. Pandoe (2003) Temperature and salinity variability in the exit passages of the Indonesian Throughflow. *Deep-Sea Res., II*, **50**, 2183–2204.

Sprintall, J. and M. Tomczak (1992) Evidence of the barrier layer in the surface layer of the tropics. *J. Geophys. Res.*, **97**, 7305–7316.

Stammer, D. (1997) Global characteristics of ocean variability estimated from regional TOPEX/Poseidon altimeter measurements. *J. Phys. Oceanogr.*, **27**, 1743–1769.

Stommel, H. M. (1960) Wind-drift near the equator. *Deep-Sea Res.*, **6**, 298–302.

Swallow, J. C. (1983) Eddies in the Indian Ocean. In: A. R. Robinson (ed.), *Eddies in Marine Science*, Springer-Verlag, New York, pp. 200–218.

Swenson, M. S. and D. V. Hansen (1999) Tropical Pacific Ocean mixed layer heat budget: The Pacific cold tongue. *J. Phys. Oceanogr.*, **29**, 69–82.

Tilberg, C. E., H. E. Hurlburt. J. J. O'Brien, and J. F. Shriver (2001) The dynamics of the East Australian Current system: The Tasman Front, the East Auckland Current, and the East Cape Current. *J. Phys. Oceanogr.*, **31**, 2917–2943.

Tilburg C. E., H. E. Hurlburt, J. J. O'Brien, and J. F. Shriver (2002) The dynamics of the East Australian Current system: The Tasman Front, the East Auckland Current, and the East Cape Current. *J. Phys. Oceanogr.*, **31**, 2917–2943.

Tomczak, M. and J. S. Godfrey (1994) *Regional Oceanography: An Introduction*. Pergamon Press, Oxford, 422 pp.

Trasviña, A. (1995) Offshore wind forcing in the Gulf of Tehuantepec, Mexico: The asymmetric circulation. *J. Geophys. Res.*, **96**, 12599–12618.

Tsai, P. T. H., J. J. O'Brien, and M. E. Luther (1992) The 26-day oscillation observed in satellite sea surface temperature measurements in the equatorial western Indian Ocean. *J. Geophys. Res.*, **97**, 9605–9618.

van Oldenborgh, G. J. (2000) What caused the onset of the 1997–98 El Niño? *Mon. Wea. Rev.*, **128**, 2601–2607.

Vecchi, G. A. and D. E. Harrison (2000) Tropical Pacific sea surface temperature anomalies, El Niño, and westerly wind bursts. *J. Climate*, **13**, 1814–1830.

Vinayanchandran, P. N. and T. Yamagata (1998) Monsoon response of the sea around Sri Lanka: Generation of thermal domes and anticyclonic vortices. *J. Phys. Oceanogr.*, **28**, 1946–1960.

Waliser, D. E., R. Murtugudde, and L. E. Lucas (2003) Indo-Pacific ocean response to atmospheric intraseasonal variability. Part I: Austral summer and the Madden–Julian Oscillation. *J. Geophys. Res.*, **108**, 3160, doi:10.1029/2003JC001620.

Waliser, D. E., R. Murtugudde, and L. E. Lucas (2004) Indo-Pacific ocean response to atmospheric intraseasonal variability. Part 2: Boreal summer and the intraseasonal oscillation. *J. Geophys. Res.*, **109**, C03030, doi:10.1029/2003JC002002.

Wang, W. and M. J. McPhaden (1999) The surface-layer heat budget in the equatorial Pacific Ocean. Part I: Mean seasonal cycle. *J. Phys. Oceanogr.*, **29**, 1812–1831.

Webster, P. J. and R. Lukas (1992) TOGA-COARE: The coupled ocean–atmosphere response experiment. *Bull. Amer. Meteor. Soc.*, **73**, 1377–1416.

Webster, P. J., E. F. Bradley, C. W. Fairall, J. S. Godfrey, P. Hacker, R. A. Houze, R. Lukas, Y. Serra, J. M. Hummon, T. D. M. Lawrence *et al.* (2002) The JASMINE pilot study. *Bull. Amer. Meteorol. Soc.*, **83**, 1603–1630.

Webster, P. J., A. M. Moore, J. P. Loschnigg, and R. R. Leben (1999) Coupled ocean–atmosphere dynamics in the Indian Ocean during 1997–98. *Nature*, **401**, 356–360.

Weidman, P. D., D. L. Mickler, B. Dayyani, and G. H. Born (1999) Analysis of Legeckis eddies in the near-equatorial Pacific. *J. Geophys. Res.*, **104**, 7865–7887.

Weisberg, R. H., A. M. Horigan, and C. Colin (1979) Equatorially-trapped variability in the equatorial Atlantic. *J. Mar. Res.*, **37**, 67–86.

Weisberg, R. H. and T. Y. Tang (1983) Equatorial ocean response to growing and moving wind systems, with application to the Atlantic. *J. Mar. Res.*, **41**, 461–486.

Weisberg, R. H. and C. Wang (1997) Slow variability in the equatorial west-central Pacific in relation to ENSO. *J. Climate*, **10**, 1998–2017.

Weller, R. A. and S. P. Anderson (1996) Surface meteorology and air–sea fluxes in the western equatorial Pacific warm pool during the TOGA coupled ocean–atmosphere response experiment. *J. Climate*, **9**, 1959–1990.

Willson, H. R. and N. W. Rees (2000) Classification of mesoscale features in the Brazil–Falkland Current confluence zone. *Prog. Oceanogr.*, **45**, 415–426.

Wu, L., Z. Liu, and H. E. Hurlburt (2000) Kelvin wave and Rossby wave interaction in the extratropical–tropical Pacific. *Geophys. Res. Lett.*, **27**, 1259–1262.

Wyrtki, K. (1973) An equatorial jet in the Indian Ocean. *Science*, **181**, 262–264.

Yoshida, K. (1959) A theory of the Cromwell Current (the equatorial undercurrent) and of equatorial upwelling. *J. Oceanogr. Soc. Jap.*, **15**, 159–170.

Yu, L. S. (2003) Variability of the depth of the 20°C isotherm along 6°N in the Bay of Bengal: Its response to remote and local forcing and its relation to satellite SSH variability. *Deep-Sea Res.-II*, **50**, 2285–2304.

Yu, Z. J., J. P. McCreary, and J. A. Proehl (1995) Meridional asymmetry and energetics of tropical instability waves. *J. Phys. Oceanogr.*, **25**, 2997–3007.

Yu, Z. J. and P. S. Schopf (1997) Vertical eddy mixing in the tropica upper ocean: Its influence on zonal currents. *J. Phys. Oceanogr.*, **27**, 1447–1458.

Zebiak, S. E. (1989) On the 30–60 day oscillation and the prediction of El Niño. *J. Climate*, **2**, 1381–1387.

Zebiak, S. E. and M. A. Cane (1987) A model El Niño-Southern Oscillation. *Mon. Wea. Rev.*, **115**, 2262–2278.

Zhang, C. (1996) Atmospheric intraseasonal variability at the surface in the tropical western Pacific Ocean. *J. Atmos. Sci.*, **53**, 739–758.

Zhang, C. (1997) Intraseasonal variability of the upper-ocean thermal structure observed at 0° and 165°E. *J. Climate*, **10**, 3077–3092.

Zhang, C. (2001) Intraseasonal perturbations in sea surface temperatures of the equatorial eastern Pacific and their association with the Madden–Julian Oscillation. *J. Climate*, **14**(6), 1309–1322.

Zhang, C. D. and J. Gottschalck (2002) SST anomalies of ENSO and the Madden–Julian oscillation in the equatorial Pacific. *J. Climate*, **15**, 2429–2445.

Zhang, C. and M. J. McPhaden (2000) Intraseasonal surface cooling in the equatorial western Pacific. *J. Climate*, **13**, 2261–2276.

Zhang, C., H. H. Hendon, W. S. Kessler, and A. J. Rosati (2001) A workshop on the MJO and ENSO: Meeting summary. *Bull. Amer. Meteorol. Soc.*, **82**, 971–976.

Zhang, K. Q. and L. M. Rothstein (1998) Modeling the oceanic response to westerly wind bursts in the western equatorial Pacific. *J. Phys. Oceanogr.*, **28**, 2227–2249.